2004

High Quality ZnO Epitaxial Grown By Plasma Assisted Molecular Beam Epitaxy

Yun Zhang
Virginia Commonwealth University

HIGH QUALITY ZNO EPITAXIAL GROWN BY PLASMA ASSISTED MOLECULAR BEAM EPITAXY

A thesis submitted in partial fulfillment of the requirements for the degree of Master of Science in Electrical Engineering at Virginia Commonwealth University

BY

YUN ZHANG

B.S., Tsinghua University, 1998

M.S., Tsinghua University, 2001

Director: Dr. Hadis Morkoc, Founders Professor

in Department of Electrical Engineering

Virginia Commonwealth University

Richmond,Virginia

December, 2004

ACKNOWLEDGEMENTS

I would like to thank my advisor, Professor Hadis Morkoç, for his financial support and guidance during the course of work.

I would like to extend many thanks to Professor Dan Johnstone and Professor Michael Reshchikov for their helpful suggestions and involvement.

I have benefited greatly from many member of our research group. Among them are Dr. C. Liu, Dr. Y. Feng, Dr. Y. Moon, Dr. S. Cho, Dr. Y. Alivov, X.,Gu, J. Xie, L., He, Y. Fu, B. Xiao et al.

Finally, I would like to thank my wife and our family for their support and encouragement.

Table of Contents

ACKNOWLEDGEMENTS ..... **ii**

Table of Contents ..... **iii**

ABSTRACT ..... **v**

Chapter 1 Introduction **1**

Chapter 2 Theoretical Background **4**

2.1 STRUCTURE AND PROPERTIES OF ZINC OXIDE 4

2.2 MBE 7

2.3 Characterization 16

Chapter 3 growth and characterization of ZnO films on c-plane (0001) sapphire **20**

3.1 Introduction 20

3.2 Theoretical Background 20

3.3 ZnO growth experiments and discussions 31

Chapter 4 growth and characterization of ZnO films on epi-GaN **45**

4.1 Introduction 45

4.2 Experimental procedures 47

4.3 Results and discussions 48

Conclusion 64

List of reference 66

ABSTRACT

HIGH QUALITY ZNO EPITAXIAL GROWN

BY PLASMA ASSISTED MOLECULAR BEAM EPITAXY

By Yun Zhang, Master of Science

A thesis submitted in partial fulfillment of the requirements for the degree

of Master of Science in Electrical Engineering at Virginia Commonwealth University

Virginia Commonwealth University, 2004

Major Director: Dr. Hadis Morkoç,

Founders Professor in Department of Electrical Engineering

Described in this thesis are the growth and characterization of high quality ZnO epitaxy layers.Zinc oxide (ZnO) epitaxy layers were grown on sapphire and epi-GaN substrates respectively, using plasma assisted molecular beam epitaxy (MBE) . Various growth conditions, such as growth temperature, II/VI ratio, and buffer layers, were employed to optimize the quality of the ZnO film. The subsequent characterization of the

films was carried out to evaluate the surface, optical and crystalline properties of the film, using AFM, SEM, PL and XRD techniques. It was found out that the high quality of the ZnO film was grown on epi-GaN substrates under the Low temperature of ~ 300°C, flash annealing up to ~680°C, followed by high temperature growth at ~600°C.

Chapter 1 Introduction

Zinc oxide (ZnO), naturally as the mineral zincite, has been known since the time of the ancients[1]. Historically it is used as a white pigment in watercolors and paints, and also an activator in the rubber industry. In research, it has been the subject of extensive studies as a unique material, which exhibits good semiconducting, piezoelectric and pyroelectric multiple properties. Only recently, has ZnO been receiving continued interest as a wide-gap semiconductor compound because the developing practical short-wavelength semiconductor diode lasers are needed by the huge commercial market[2, 3][2, 4-7] The reasons lie not only in its wide band gap energy (3.37 eV) as a semiconductor, but also in its large excitation binding energy (60 meV) compared to other semiconductors such as GaN (25 meV) and ZnSe (22 meV). To achieve efficient excitonic laser action at room temperature, the binding energy of the exciton must be much greater than its thermal energy at room temperature (26 meV) [8], and only ZnO has such advantage to allow for significant excitonic emission at/above room temperature. As a result, these properties provide the possibility of practical ZnO lasers with low thresholds even at high temperature.

As a promising material to be used in optoelectronic device or other application, high

quality single crystal thin films of ZnO with structures as low as monolayer dimensions are required. Consequently, several problems arise: How to produce the high-quality single crystal thin films on certain substrates for such application? What growth technique should be employed considering the impurity, doping, and the degree of growth control? Which substrate is most compatible with this ZnO film to obtain high quality ZnO films, etc.?

Therefore, to address some of these issues, this study will focus on the growth of ZnO films on sapphire and GaN using plasma assisted molecular beam epitaxy method (MBE). MBE, as a means of growing high-purity epitaxial layers of compound semiconductors with high degree of control, can meet the requirement of the high quality single crystal thin films, making possible in theory the growth of high-quality layers on abrupt interfaces, and precisely controlling the thickness, doping and composition.

The research on the growth of ZnO using MBE has been extensively reported. However, the crystal quality of the ZnO films still needs to be improved for their future application in semiconductor devices. To solve this problem, work needs to be done both theoretically and experimentally to improve the quality of the film.

Therefore, the theoretical background of controlling parameters of ZnO growth using MBE will be addressed in the second chapter, followed by the experimental work on the growth of ZnO films on different substrates in the third and the fourth chapters.

The third chapter reports the growth of ZnO films on c-plane of the sapphire along the (0001) orientation and the corresponding characterization, in which the rotation domains, growth mode, surface morphology and crystal quality were analyzed. In addition, the relationship between the annealing temperature and ZnO quality was discussed.

Although sapphire is the most common substrate for ZnO film growth, the large lattice mismatch hinders the high quality ZnO epilayer growth. Based on the above consideration, GaN is a good candidate substrate for ZnO growth due to its similar crystal structure and thermal properties. Thus in the fourth chapter, the characterization and growth of ZnO films on epi-GaN were studied with the optimization of buffer layer and temperature, followed by a discussion on the heterointerface between ZnO films and GaN layers, and an analysis of the crystal and optical properties through AFM, SEM, PL and XRD techniques.

Chapter 2 Theoretical Background

2.1 STRUCTURE AND PROPERTIES OF ZINC OXIDE

2.1.1 Crystallography of Zinc Oxide

Like most of the II–VI group binary compound semiconductors, zinc oxide has two polytypes: cubic zinc-blende and hexagonal wurtzite structure[9] as shown in Figure 1.

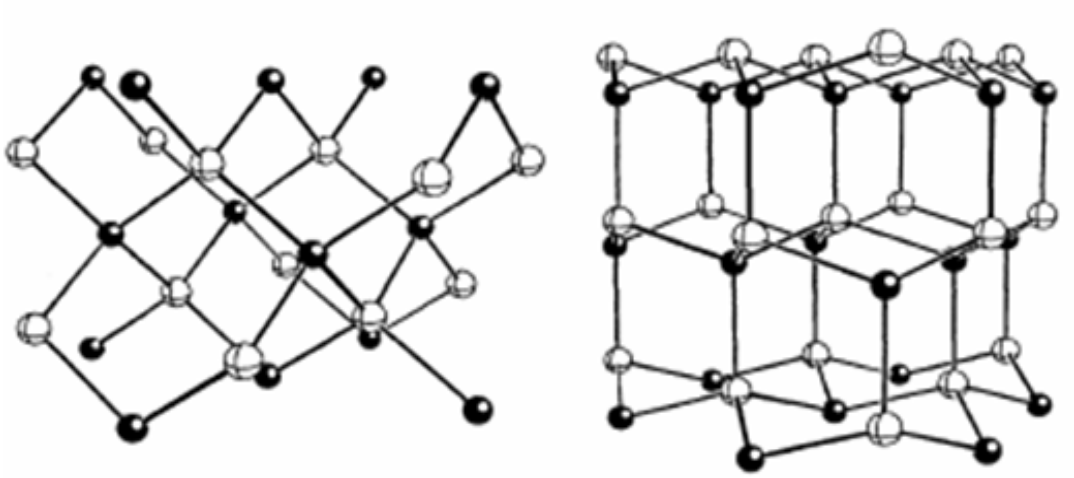

Figure 1. Crystal structures of ZnO : Cubic zinc blende and hexagonal wurtzite

In the cubic zinc blende structure, zinc atoms reside at all the corners and face centers of the cube; oxygen atoms take up four of the tetrahedral sites. In the hexagonal

wurtzite structure, each anion is surrounded by four cations at the corners of a tetrahedron, and this tetrahedral coordination is a typicaly sp^3 covalent bonding. The two useful wurtzite lattice parameters are a (3.249nm), c (5.205nm) and the ratio of c/a=1.60 (thesedata vary in a small range since it was determined by different methods). Similarly, GaN is a closely lattice-matched materials comparing to ZnO with a lattice mismatch of only 1.8%, and has isomorphic crystal structure, which is why GaN is a good candidate as a substrate to grow ZnO films. Details on the substrate of GaN will be discussed in chapter 4. The wurtize structure is composed of two interpenetrating hexagonal close-packed sublattices, with each sublattice containing four atoms. These two sublattices displace with respect to each other along the three-fold c-axis. The four nearest neighbors and twelve next neighbors have the same bond distance in both zinc blende and wurtzite structure. However, the stacking sequences of the closed-packed diatomic planes are different, i.e., in wurtzite structure, the stacking order of (0001) plane could be AaBbAaBb… in the <0001> direction, but for zinc blende structure, the order for the (111) planes along the $\langle 111 \rangle$ direction is AaBbCcAaBbCc.....

2.1.2 Electrical and optical properties

The electrical properties of ZnO are excellent due to its large band gap ($E_g = 3.37eV$). To make any type of device technology into practice with ZnO, it is important to have control over the concentration of intentionally introduced impurities

(dopants) which affect the electrical properties of ZnO. The dopants determine whether the current is carried by electrons or holes. In general, because the dopants introduce the energy levels close to the energy band which are easily ionized, the dopants are shallow level impurities. For the deep level defects or impurities, they are often introduced by unintentional impurities which have harmful effect on the properties of the material. For instance, they may be resulted from structure defects in the Zn crystal lattice or introduced from the contamination during the growth process.

This band gap can be changed by introducing divalent substitution on the cation site to produce a heterostructure. For example, cadmium doping can lower the band gap to ~3.0 eV, while magnesium doping can increase the band gap to ~4.0 eV[10]. Because of the presence of intrinsic defects, such as O vacancies and Zn interstitials, ZnO in a wurtzite structure is naturally a *n*-type semiconductor with high electron densities. The intrinsic defect level that leads to *n*-type doping lies approximately 0.01 – 0.05 eV below the conduction band.

The optical properties of ZnO are usually described with the intrinsic direct band gap through photoluminescence (PL), photoconductivity, and absorption. Details of PL will be discussed in chapter 4.

Overall, the properties (shown in Table 1[10]) include high breakdown voltages, low noise generation, and operability at high temperature and high power. With a direct wide

bandgap energy of 3.37 eV at room temperature and free-exciton binding energy of 60 meV, ZnO has become a great promising material for optoelectronics applications such as blue-and ultraviolet (UV) light emitters and UV detectors operating at high temperatures, and also a candidate to realize low-threshold excitonic ZnO lasers.

Table 1. Properties of wurtzite ZnO[10]

Property	Value
Lattice parameters at 300 K:	
a_0	0.32495 nm
c_0	0.52069 nm
a_0/c_0	1.602 (1.633 for ideal hexagonal structure)
u	0.345
Density	5.606 g/cm^3
Stable phase at 300 K	wurtzite
Melting point	1975°C
Thermal conductivity	0.6, 1-1.2
Linear expansion coefficient (/°C)	a_0: 6.5 × 10^{-6}, c_0: 3.0 × 10^{-6}
Static dielectric constant	8.656
Refractive index	2.008, 2.029
Energy gap	3.4 eV (direct)
Intrinsic carrier concentration	<10^6/cm^3
Exciton binding energy	60 meV
Electron effective mass	0.24
Electron Hall mobility at 300 K for low *n*-type conductivity	200 cm^2/V·s
Hole effective mass	0.59
Hole Hall mobility at 300 K for low *p*-type conductivity	5-50 cm^2/V·s

2.2 MBE

Molecular beam epitaxy (MBE) denotes the epitaxial growth of compound semiconductor films, which involves the reaction of one or more thermal molecular

beams with a crystalline surface under ultra-high vacuum condition. It was developed in the early 1970s and has evolved into a popular technique to grow II/VI compound semiconductors as well as several other materials[11]. Because the layer grows in the ultra high vacuum (UHV) controlled environment, there will be a minimal incorporation of contaminants such as carbon and oxygen. Another obvious advantage of MBE is that it allows making compound semiconductor materials with great precision and purity, and gives more design options. For example, MBE allows for good control of interfaces ,thickness, doping, and composition to obtain high quality ZnO films. Therefore, it has become a valuable tool in the development of sophisticated electronic and optoelectronic devices [12].

2.2.1 MBE principle and apparatus

Figure 2 shows the MBE growth mechanism. When Zn and O atoms arrive at the sapphire substrate surface, they may undergo absorption to the surface, surface migration, incorporation into the crystal lattice, and thermal desorption processes. It will depend strongly on the temperature of the substrate which process dominates the growth. High quality crystal can be only achieved in a moderate range of temperatures, at which the atoms will have sufficient energy to move to the proper position on the surface and will be incorporated into the growing crystal.

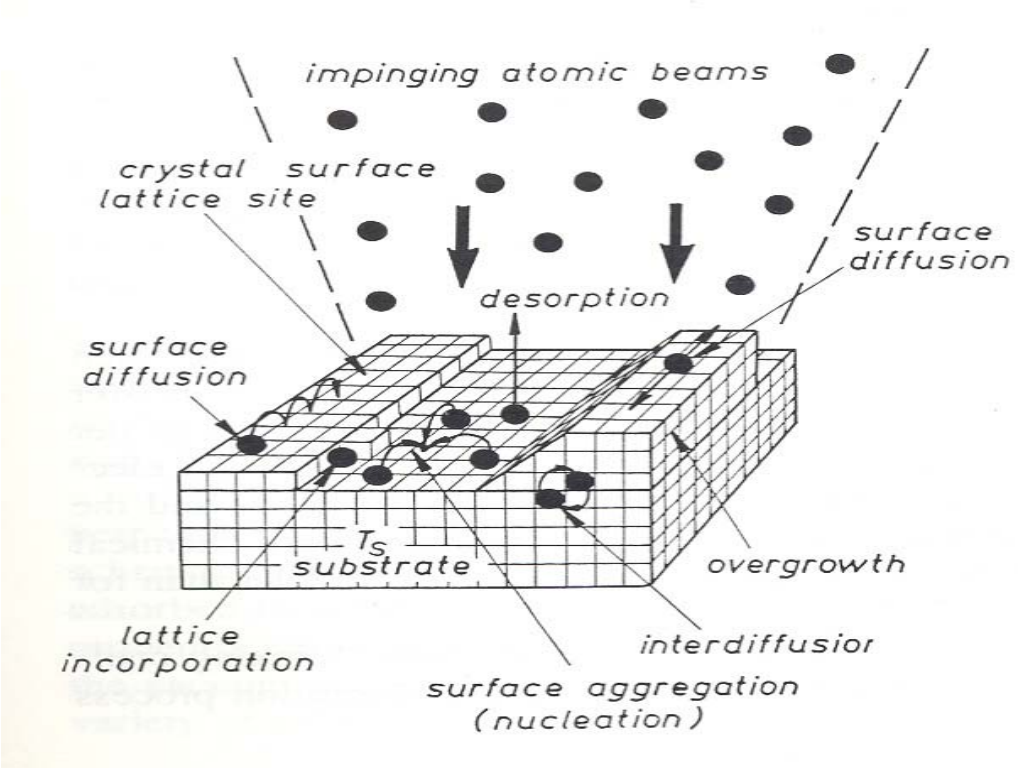

Figure 2. Schematic diagram of MBE growth [13]

Virginia Commonwealth University boasts the Riber 3200 MBE systems with reflection-high energy electron diffraction (RHEED) (shown in Fig 3). This system consists of two main vacuum chambers: a growth chamber (the pressure is at ~10^{-8}- ~10^{-9} torr at idle status) and a load chamber (the pressure is at ~10^{-7} torr). The load chamber is used to transfer samples into/out from the vacuum environment while maintaining the vacuum integrity. It can also be used for sample storage in vacuum condition. The samples are transferred via a magnetically coupled transfer rod which can be rotated and

shifted smoothly. The growth chamber of a general MBE system and subsystems are illustrated in Figure 4[10]. It includes several vacuum effusion cells for the evaporation of various atomic or molecular materials. Each cell has a shutter for on/off control of each beam. The substrate holder can be rotated to assure that each material is distributed across the wafer as uniformly as possible. RHEED equipped in the growth chamber is one of the most useful tools for *in-situ* monitoring of the growth. It can be used to calibrate growth rates and the substrate temperature, to monitor the arrangement of the surface atoms, to adjust radio frequency (RF) O flux, to produce feedback on surface morphology, and to provide information about growth kinetics. The RHEED gun emits ~10KeV electrons at high voltages. These electrons reflect from the surface, strike a phosphor screen, and then form an image consisting of a specular reflection and a diffraction pattern which implies the surface crystallography. Since the electrons strike the surface with a very shallow angle (~0.5-2 degrees), the pattern is very sensitive to surface structure. A camera with computer control is employed to monitor the screen and record live pictures or measure the intensity of a given pixel as a function of time. Some other accessories are mounted in the growth chamber, including an ion gauge to detect the pressure in the chamber and a thermocouple to monitor the temperature, etc.

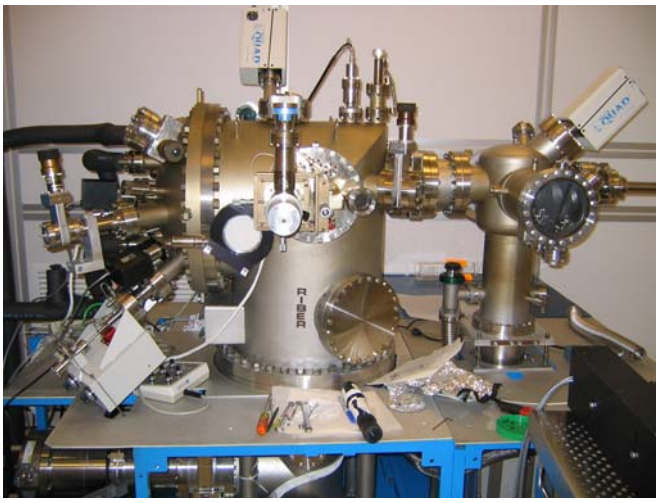

Figure 3. Riber 3200 MBE system in VCU

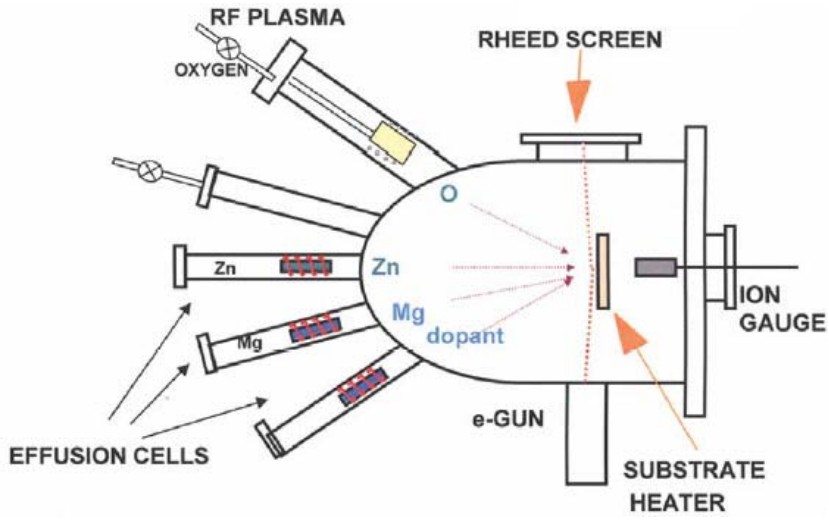

Figure 4. Schematic of MBE growth system

The solid sources in this Riber 3200 system are pure elements Zn and Mg (for doping) which are loaded in the effusion cells. At room temperature, these charges are solid; when heated in the effusion cell, the charges generate gaseous atomic or molecular beams to the substrate wafer, whose flux (the effective beam pressure or the gas flow rate)

change with the effusion cell temperature. The relation between flux F and temperature is given by[11]:

$$F = \frac{P_{(T)}a}{mL^2\sqrt{2\pi mkT}} molecule/cm^2 \sec$$

where $P_{(T)}$ is the equilibrium pressure at the cell temperature T, ***a*** is the area of the cell aperture, ***L*** is the distance to the substrate and *m* is the mass of the effusion species.

Using this expression, the Ga and Mg flux can be calculated approximately at a given temperature in the experiment.

The Knudsen cell utilizes the principle of molecular effusion (demonstrated by Knudsen in 1909): materials to be deposited is heated to provide a suitable vapor pressure in an isothermal enclosure; molecular effusion intensity distribution from an aperture in the bottom of the cell follows the cosine rule; the deposition rate is extremely stable and is determined by the temperature of the furnace which can be accurately controlled.

There is a shutter lying on the top of the effusion cell, which can "shut off" the beam. Actually, when the shutter is closed, the gas is not enclosed in the cell completely, but is deflected away from the substrate and pumped away through the growth chamber.

O element, another component in ZnO is obtained from pure oxygen, which acts as the gas source in this experiment. A standard gas handling system connects the external gas canister to the growth chamber. Beam fluxes change almost immediately by

adjusting the gas flow valves. When the valve is closed, no charge material enters the chamber. The sources are easily refilled without breaking vacuum system of the growth chamber. The add-on Knudsen cells used in this Riber system, need 13.56 MHz high brightness RF plasma to produce an atomic species beam from oxygen.

2.2.1 MBE growth parameters

a) Growth temperature

The growth temperature is one of the crucial parameters to achieve high quality ZnO films. According to the MBE technical principle discussed above, several processes occur when molecules arrive at the substrate, including adsorption, migration on the substrate surface, interaction with other atoms, incorporation into the crystal, or desorption, all of which are affected by the growth temperature (the substrate temperature). Only at high temperatures, the arriving Zn and O atoms have sufficient energy to move around on the surface and deposit on their correct bonding positions. However, if the temperature is too high, these atoms may be re-evaporated from the surface, which leads to low growth rate. If the temperature is too low, these atoms cannot find the correct positions without high enough energy, which leads to high grow rate but poor crystal quality of the ZnO films. Therefore, the optimization of growth temperature is a key procedure to obtain high quality ZnO films.

b) II/VI ratio

Another important parameter to control the ZnO growth is the II/VI element ratio.Under different conditions, MBE-grown ZnO exhibits three distinct growth regimes as shown in Figure 5 [14, 15]: O-rich (II/VI <1), stoichiometric (II/VI =1) and Zn-rich (II/VI>1). When the active oxygen flux is kept constant during the growth, the II/VI ratio varies with the effusion cell temperature. The higher the cell temperature (zinc), the higher the II/VI ratio. The growth rate increases as the Zn flux rises under O-rich conditions and reaches the saturation under stoichiometric conditions. The II/VI ratio is responsible for the electrical, optical and other properties of ZnO films. High crystal quality ZnO was obtained under the stoichiometric flux condition together with the lowest dislocation density and the highest electron mobility (~130$cm^2V^{-1}s^{-1}$) compared to the ZnO films grown under nonstoichiometric flux conditions[14, 15].

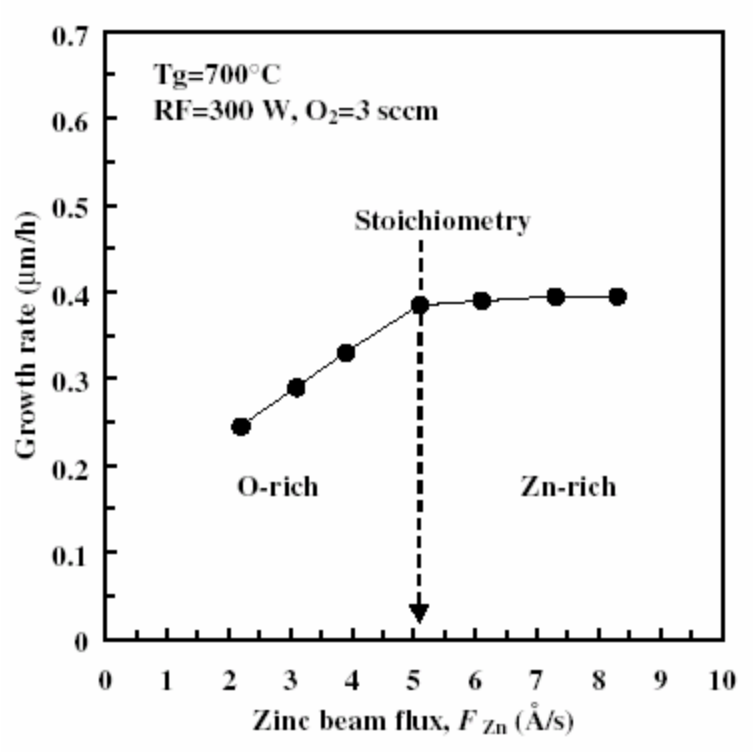

Figure 5. Growth rate of ZnO layers against Zn beam flux, F_{Zn}[14, 15]

c) Substrate

Substrate selection is important to expitaxial growth. Generally close-matched substrates are used by most research groups to reduce the film stress and dislocations in epitaxial films. The sapphire substrate is commonly used for ZnO heteroepitaxial growth on the (0001) orientation. However, there is a large lattice mismatch (18%) between the ZnO epilayer (a = 0.3250 nm, c = 0.5213 nm) and the sapphire (a = 0.4754 nm, c = 1.299 nm) substrate, resulting in large crystal mosaics, high residual carrier concentrations and low mobility[16], thereby hindering its use for optoelectronic applications. As a

consequence, the substrate material with smaller lattice mismatch is better for ZnO growth.

GaN is a good candidate since it is a closely lattice-matched material to ZnO with a lattice mismatch of only 1.8%, and also a smaller thermal mismatch, compared to ZnO on Al_2O_3. The details will be discussed in Chapters 3 and 4.

Other parameters, such as pretreatment process, polarity properties, etc., also affect the properties of ZnO films and the optimization of these conditions are needed for high quality ZnO films.

2.3 CHARACTERIZATION

Several techniques are employed to characterize the quality of ZnO films: *in-situ* RHEED observation, *ex-situ* atomic force microscope (AFM), X-ray diffraction (XRD), scanning electron Microscopy (SEM) and photoluminescence (PL) measurement. RHEED is used to monitor the growth mode and surface during the MBE growth; AFM and SEM are used to observe the surface morphology.

XRD is used to characterize crystal forms and the residual impurities in the ZnO films. Basic XRD measurements made on thin film samples include the rocking curve measurement and the precise lattice constants measurements. According to Bragg law:

$$n\lambda = 2d\sin\theta$$

where *λ: wavelength, d : the spacing of the layers, θ: the incident angle of the photons.*

the diffraction for a given plane and wavelength not only takes place over the zero angular range defined, but also over a small finite range, so this range is just the rocking curve width. Therefore, the rocking curve measurements are made by doing a θ scan at a fixed 2θ angle, the full width at the half maximum (FWHM) is inversely proportionally to the dislocation density in the film and used a gauge of the quality of the film[17]. Thus the narrower the peak of the FWHM and the stronger the intensity of XRD curves are, the better the crystal quality would be.

From the 2θ - θ scanning, precise lattice constants measurements, the information about lattice mismatch between the film and the substrate are provide and therefore it is indicative of strain and stress.

Luminescence is a process through which a matter generates non-thermal radiation. Therefore it can be used to characterize particular luminescent materials. Photoluminescence (PL) is one of the most useful optical methods in the optoelectronic semiconductor research, which is sufficiently powerful and sensitive to probe the impurities and defects in semiconductors. A given impurity produces a series of characteristic spectra, through which the impurity type can be identified. In general, several different impurities can be observed in a single PL spectrum. In addition, the half widths of PL peaks are used as a means to evaluate the crystal quality. However, this analysis based on the half widths of PL peaks could not produce highly quantitative

results.

Luminescence may involve radiation, accompanied by emittance of photons when an electron drops from an upper energy level to a lower level, either in intrinsic band states or impurity levels. There are several different types of radiations. To analyze the PL spectrum, we need to understand these radiations clearly.

(1) Free-to-bound transition

Free-to-bound transition is between intrinsic band and impurity state, which may occur between impurity and one of the bands, such as conduction band to acceptor or donor to valence band, with momentum and energy conserved even in indirect band gap materials.

(2) Band-to-band transitions:

Band-to-band transitions often occur in direct band gap materials and involve free electrons and holes. The electron-hole pairs have high probability of recombination rate.

(3) Donor-acceptor pairs (DAP) recombination

DAP transition is between donor and acceptor levels, where electrons and holes can take place at D^+ and A^- sites to produce neutral D^0 and A^0 centers. For balance, some of the electrons on the neutral donors will recombine rediatively with holes on the neutral acceptors.

(4) Free exciton transitions

Free exciton illustrates the lowest energy of intrinsic of excitation for electron and holes which are in the pure materials and at low excitation density. The free exciton state can be described by the Wannier-Mott approximation where the carriers are independent, and the oppositely charged particles interact with each other by Coulomb force. The energy of free exaction is given by

$$E_n = \frac{2\pi^2 m^* e^4}{h^2 \varepsilon^2 n^2}$$

where m* is the reduced mass, n is the quantum number, ε is the dielectric constant and h is the Plank constant. The free exciton leads to a decrease in the energy of electron-hole pairs by $h\nu = E_g - E_n$

For high crystal quality bulk ZnO, there is a broad peak at 3.2eV with FWHM about 100 meV at room temperature; at low temperature, the neutral shallow donor-bound exciton will dominate at 3.42 eV due to the presence of donor sources coming from unintentional impurities or shallow defects. These properties can be used to estimate the binding energy of the donors.

Chapter 3 growth and characterization of ZnO films on c-plane (0001) sapphire

3.1 INTRODUCTION

The sapphire substrate is widely used for ZnO heteroepitaxial growth and has shown promising optical properties in spite of the crystal quality. In this chapter, the growth of ZnO films on the c-plane of sapphire along the (0001) orientation will be investigated together with its characterization.

3.2 THEORETICAL BACKGROUND

3.2.1 The advantage and disadvantage of using sapphire substrates

Homoepitaxial growth of ZnO films on ZnO substrates is most desirable; however, the prohibitive price of the commercial bulk ZnO forces researchers to find other substitutes. Among them, sapphire (α-Al_2O_3) is the most widely used substrates for heteroepitaxial growth of ZnO films due to its low cost and high crystalline quality[18].

However, there is a large misfit (about 18 %) between ZnO and sapphire, which degrades the quality of epitaxial ZnO films. Furthermore, rotation domains are often observed in ZnO films due to the complicated ZnO-Al_2O_3 interface formed by different chemical bonds, resulting in a reduced ZnO epilayer quality.

3.2.2 Sapphire lattice structure

To eliminate the influence of rotation domains to the quality of ZnO films, it is necessary to understand the origins of the rotation and thus to develop some techniques to eliminate them.

Sapphire (α -Al_2O_3) is the simplest and the only thermodynamically stable aluminum oxide. Therefore, it is considered as a prototype to understand metal oxides[4]. For the above reasons, the atomic structure of sapphire (0001 surface) has been studied extensively both theoretically and experimentally, with the focus on specifying the surface termination layer.

Sapphire has rhombohedral symmetry, with 15 atoms (three Al_2O_3 formula units) per primitive unit cell. Like all rhombohedral systems, a larger unit cell sapphire can be treated as a slightly distorted hexagonal close-packing of oxygen ions with small aluminum ions lying in some of interstices. Thus the atomic positions of sapphire are given in terms of a hexagonal cell[18].

Figure 6 shows an α-Al_2O_3 hexagonal unit cell structure parallel to the (0001) surface. Each atom locates at one of the 18 layers normal to the long axis of the cell. It has 12 aluminum layers (containing a single Al atom per unit cell per lance) and 6 oxygen layers (containing three O atoms which are arranged in an equilateral triangle). Each Al atom is bonded to six nearest O atoms in a distorted octahedron, while each O

atom is bonded to four Al atoms in a distorted sp^3 arrangement. Therefore, there are two nearest-neighbor bond lengths and they are 1.86μÅ and 1.96Å, respectively.

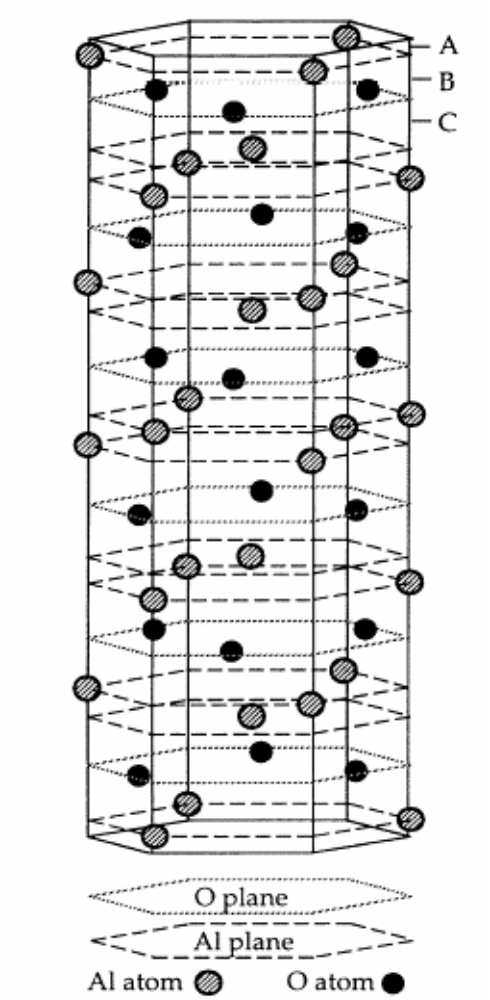

Figure 6. Bulk structure of α-Al_2O_3, solid lines show the boundaries of the hexagonal unit cell. There are only three distinct truncated bulk surfaces; there are formed by slicing the bulk with planes passing through points labeled A, B, and C, respectively. [18]

3.2.3 Rotation domains

3.2.3.1 Formation of the rotation domains

In sapphire, the oxygen layers follow hexagonal close packed (HCP) type stacking (layers are ABABAB) and are separated by c/6 along the c-axis equivalently; the aluminum layers follow face centered cubic (FCC) type stacking (layers are ABCABC…). Complicated compared to monoatomic materials, the compound sapphire has three different α-Al_2O_3 (0001) plane terminations: **a single aluminum layer**, **oxygen layer** and **a double aluminum layer**. Among the three surface structures, the Al monolayer with a three-fold symmetry has been predicted to be the most stable termination. [18]

According to the theoretical calculation, the α-Al_2O_3 with a single Al monolayer termination has a greatly contracted spacing (~85%) in the top first interlayer[19, 20]. The XRD and ion-scattering experiments support that the natural termination in α-Al_2O_3 is single Al terminated[4]. On the other hand, the less favorable O terminated surface with a six-fold symmetry can be formed after the pretreatment of plasma-excited oxygen (O*).[4]

ZnO in wurtize structure has six-fold symmetry, therefore when ZnO films grow on (0001) sapphire, ZnO (0001) surface // sapphire (0001). The epitaxial relationship between ZnO and sapphire is as the following: ZnO $[11\bar{2}0]$// sapphire $[10\bar{1}0]$ and ZnO $[10\bar{1}0]$//sapphire $[11\bar{2}0]$ along the in-plane direction, as shown in Figure 7. A 30°

rotation forms between the ZnO and sapphire α axes because the ZnO lattice aligns itself with the oxygen sublattice in sapphire[21], reducing the lattice mismatch from around 32% to 18%. Therefore, a conclusion is made that the lattice of the ZnO should be compressive in the parallel direction([00011 direction] and tensile in the perpendicular direction.

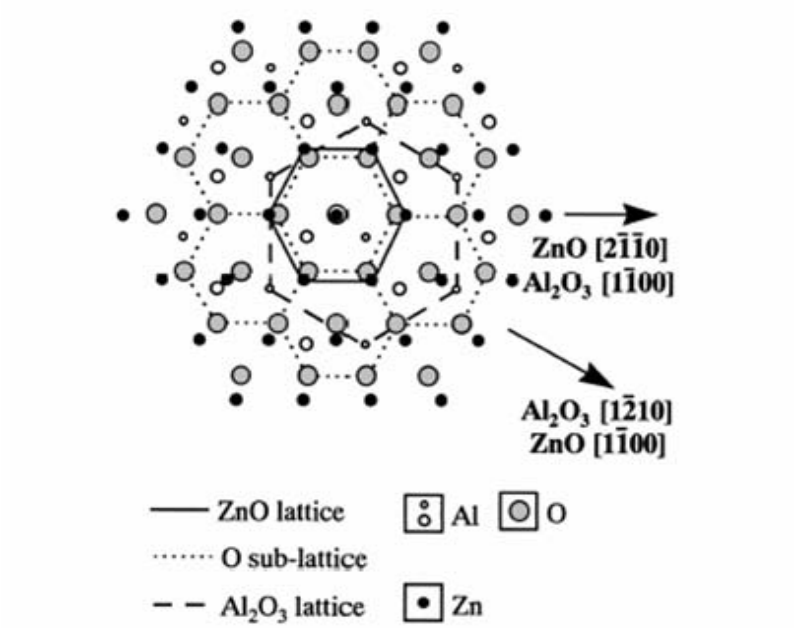

Figure 7. Schematic diagram showing the epitaxial relationship of ZnO (0001) grown on Al_2O_3 (0001)

The in-plane orientation of ZnO films to the substrate sapphire changes with different deposition temperatures. When ZnO grows on atomically flat α-Al_2O_3 (0001) place along c-axis orientation, there are two different in-plane orientations:

ZnO$[10\bar{1}0]$//sapphire $[10\bar{1}0]$ at deposition temperatures ranging from 400 to 450°C, and ZnO$[10\bar{1}0]$//sapphire $[11\bar{2}0]$ at temperatures about 800-435 °C. The XRD pole figure of the films grown at different temperatures are shown in Figure 8[22], with poles taken from ZnO $[10\bar{1}0]$ and sapphire $[10\bar{2}0]$ planes. When deposition temperatures are 400-450°C, only ZnO$[10\bar{1}0]$//sapphire $[10\bar{1}0]$ (30°C rotation) was obtained (Figure 8(a)); when temperature goes above 500°C, ZnO film with different in-plane relation ZnO$[10\bar{1}0]$//sapphire $[10\bar{2}0]$ appears (Figure 8 (b)); and when temperature is increased to 800°C, this relation becomes dominant.

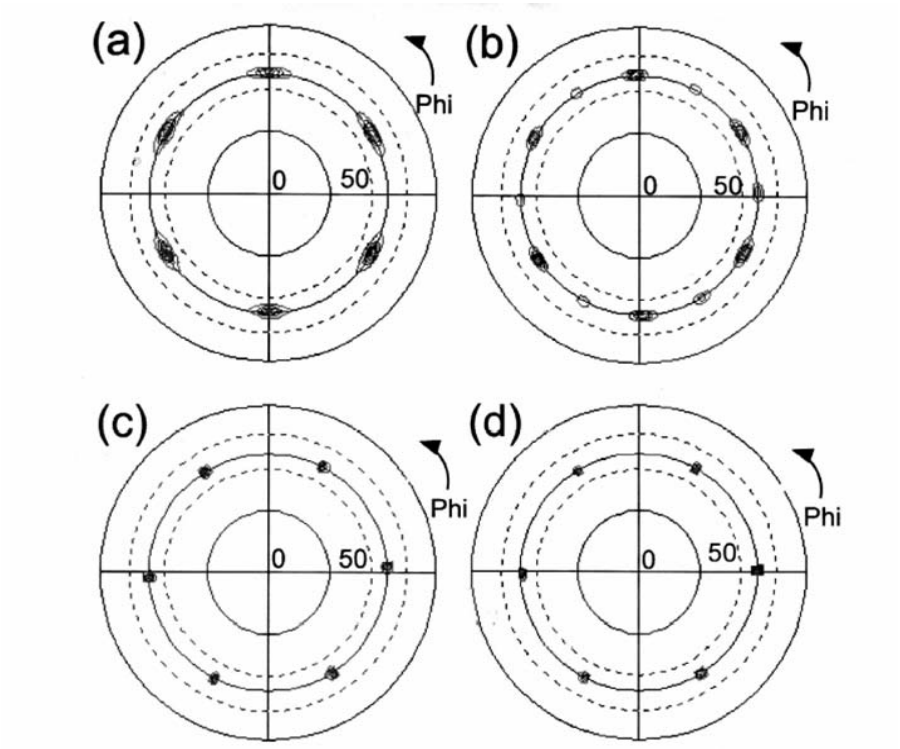

Figure 8. XRD pole figure for ZnO grown at (a) 400°C, (b) 500°C, (c) 600°C. The pole figure of sapphire (0001) substrate is shown in (d). The poles are taken for ZnO $\{10\bar{1}0\}$ and sapphire $\{11\bar{2}0\}$ planes.

3.2.3.2 Rotation domains elimination

The formation of 30° rotation domains is considered an important reason that the ZnO epilayers directly grown on sapphire (0001) has poor crystal quality. Therefore methods of eliminating the rotation domains are one of the crucial issues and they have been studied by several groups[22, 23].

The surface structure of the (0001) sapphire substrate just before the ZnO film growth has a considerable influence on the crystal quality of ZnO epi-layer. The ZnO epilayers grown on both Al- and O-terminated (0001) sapphire by using RF plasma-assisted MBE have been reported [24]. In the report, various substrate pretreatments were employed after the thermal cleaning (TC), such as atomic hydrogen (H*) and plasma-excited (O*) treatment. Furthermore, a very thin Ga metal layer was deposited to modify the sapphire surface.

Figure 9 shows the XRD pattern of ZnO films grown with different sapphire pretreatments[24].

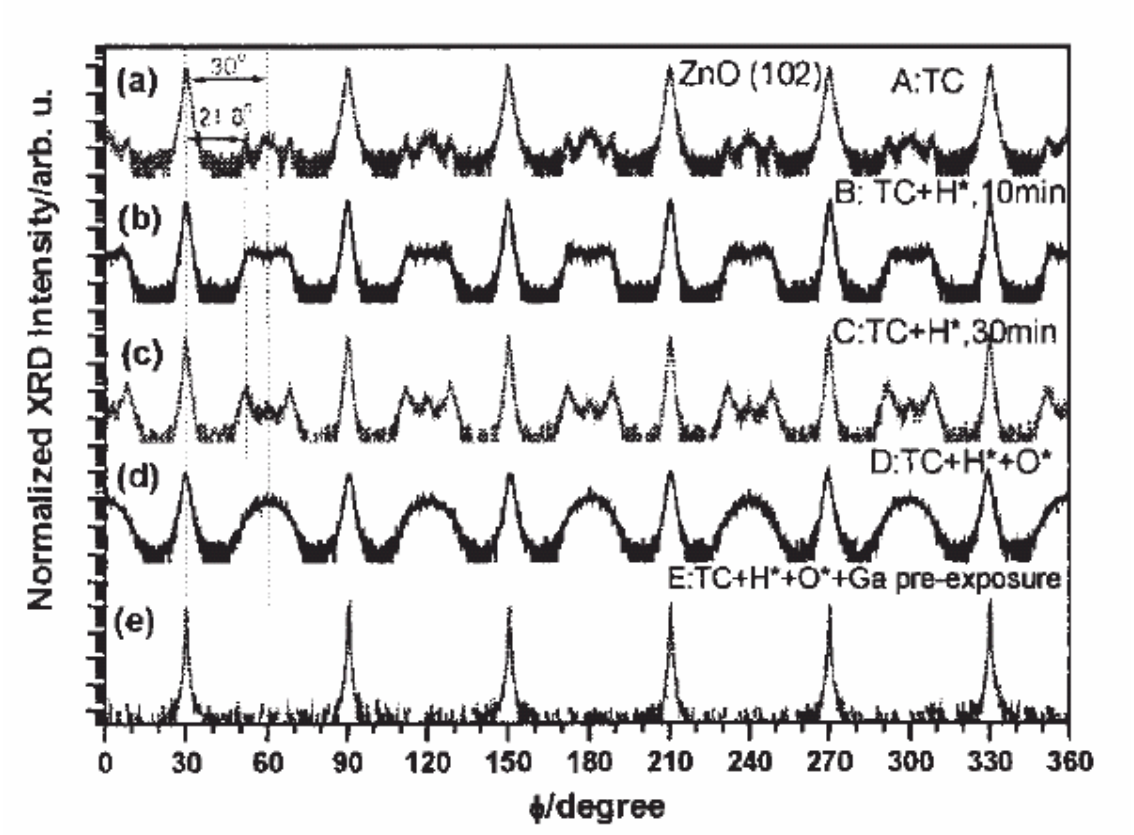

Figure 9. XRD ϕ-scans of ZnO films grown with different sapphire pretreatments showing the effect of Ga pre-exposure on the elimination of rotation domains, (a) TC only; (b) H* for 10 min after TC; (c) H* for 30 min after TC; (d) both H* and O* after TC; (e) Ga pre-exposure after TC, H* and O* pretreatment

When the ZnO layer is directly deposited on the thermally cleaned sapphire (0001) as shown in Figure 9 (a), three types of domains formed: (i) main domains with ordinary orientation relationship ($ZnO[11\bar{2}0]$//sapphire $[10\bar{1}0]$); (ii) domains with in-plane 30° rotation from the main domains along c-axis ($ZnO\,[11\bar{2}0]$ //sapphire $[11\bar{2}0]$); (iii) domains rotated by 21.8° from the main domains ($ZnO[11\bar{2}0]$//sapphire$[53\bar{8}0]$)[24].

When ZnO films grew on sapphire (0001) with H* pretreatment after thermal

cleaning, also three types of domains can be observed, as shown in Figure 9(b,c): the longer H* pretreatment time, the stronger peak intensities, the two peaks at 21.8° and 30° are more well-resolved.

The mechanism could be explained by the sapphire (0001) plane surface structure. When the ZnO film is deposited on the Al-terminated sapphire, the O atoms of the first ZnO layer form bonds with Al atoms on the uppermost layer of sapphire. Because of the large O-Al bond energy and several microstructures of the topmost Al layer on sapphire (0001) surface, the ZnO film deposited on this Al-terminated surface will also follow these Al microstructures, forming the main domains. The H* pretreatment after the thermal treatment leads to the thicker Al layer on the sapphire surface since more oxygen atoms near the surface region were removed by atomic hydrogen. In addition, the Al monolayer has been considered as the most stable termination layer. Therefore, even when the sapphire substrate is thermally cleaned at a high temperature in ultrahigh vacuum, a very thin metal Al layer will be formed on the uppermost surface due to the oxygen deficiency.

On the other hand, for an O-terminated sapphire (0001) surface which can be obtained by sufficient O* pretreatment of the sapphire substrate, the O atoms will escape from the uppermost surface and leave the local region to be Al-terminated due to the instability of the O-terminated surface. As a consequence, some O atoms in the first ZnO

layer will bind to the underlying sapphire Al atoms, whereas Zn atoms in ZnO will bind to O atoms in the underlying sapphire because of the strong Al-O bond. Thus, two types of in-plane orientation relationships between the ZnO epilayer and sapphire substrate are formed: ZnO $[10\bar{1}0]$ //sapphire $[11\bar{2}0]$ (the lattice mismatch is 18.4%) and ZnO$[11\bar{2}0]$//sapphire $[11\bar{2}0]$ (the lattice mismatch is 31.8%), with a 30° rotation along the (0001) sapphire axis between these two domains.

In addition, Du et al. reported that these rotation domains were completely eliminated by Ga pre-exposure after the O* pretreatment and the result is shown in Figure 9 (e)[24].

Besides the O* pretreatment, an alternative method has been used. Wang et al. [23, 25] nitrided the sapphire to modify its (0001) surface, suppressing the rotation domains in ZnO films, at 400°C for 1 hour before the buffer layer deposition. Then 20 nm thick ZnO buffer layer was grown at 400°C and ZnO epilayer was grown at 650°C with a thickness of 1 *um*(growth rate was about 330 nm/h). The XRD ϕ-scans for the (102) plane of the ZnO films grown with and without sapphire nitridation are shown in the Figure 10[25]. For the samples without nitridation, three kinds of rotation domains exist; for the sapphire after nitridation, only one domain exists. With nitridation, O atoms were partly replaced by nitrogen atoms, thus the first layer's compostion will be AlO_xN_{1-x}. As the nitridaiton continues, the AlN layer will form. Because the AlN layer has a single domain

hexagonal structure, following ZnO would only be grown with the epitaxial relationship of $ZnO[10\bar{1}0] // AlN\ [10\bar{1}0]$.

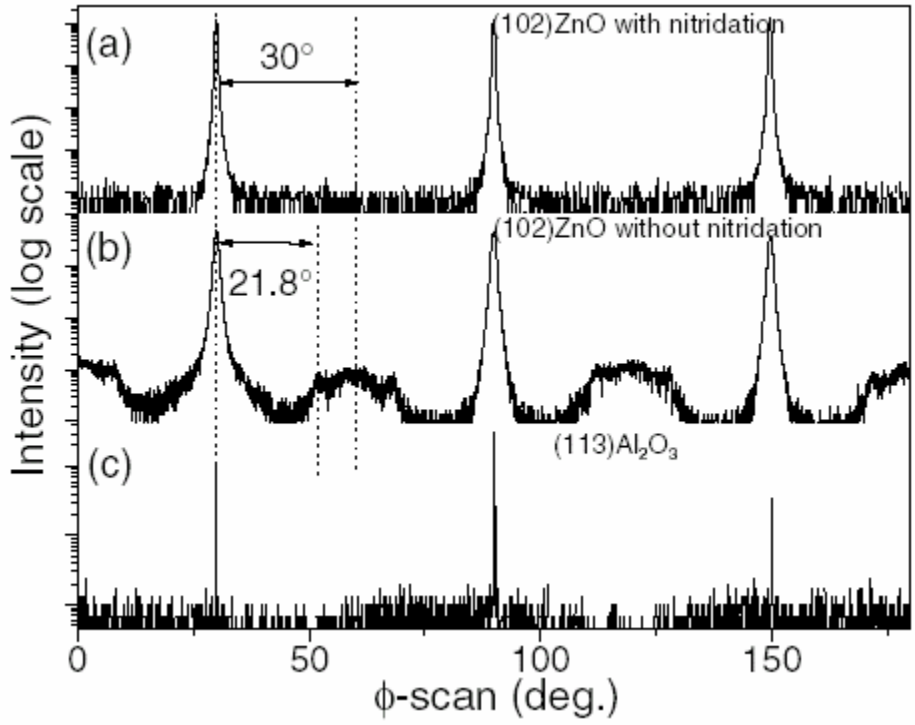

Figure 10. XRD ϕ-scan spectra. (a) (102) ZnO with sapphire nitridation; (b) (102) ZnO without sapphire nitridation; 30° and 21.8°-rotated domains are observed in this figure. (c) (113) Al_2O_3. The rotation domains are eliminated by using sapphire nitridation.

It has been confirmed that the Al_2O_3 surface becomes Al-excess after the thermal cleaning process in an ultrahigh vacuum and/or atomic H* treatment[25]. The final surface structure mainly depends on the treatment conditions, such as temperature and the procedures.

3.2.4 Other important parameters

The polarity of a wurtzite-structured ZnO has strong influence on the properties of ZnO films and their applications as devices. Hong et al grew ZnO film on the c-plane sapphire and GaN substrates by MOCVD[26]. The results show that Zn pre-exposed ZnO films have characteristics of the Zn polarity, while O-plasma pre-exposed ZnO films have a characteristic of O-polarity. Other parameters will be discussed in later analysis.

3.3 ZnO GROWTH EXPERIMENTS AND DISCUSSIONS

3.3.1 Experiment procedure and discussion

The c-plane sapphire substrates used in this study are from Saint-Gobain Crystals Company.

Surface cleaness is important to epitaxial growth, otherwise the sapphire wafer will be contaminated by the atmosphere or other sources generating crystal defects and degrading the optical and electrical properties of the epitaxial layer. AES (Auger electron spectroscopy), as one of most useful technique in MBE studies, is employed to characterize the initial substrate surface[27]. Although currently most vendors provide epi-ready wafer which were pre-cleaned in a controlled environment, the surface of the as-received sapphire is still not acceptable for high quality epitaxial growth, so the substrate needs to be pretreated before the growth.

The detailed procedures employed are as follows:

First, the substrate was rinsed for 3 minutes each in acetone, methanol and deionized (DI) water. The above rinsing steps were repeated three times for the degreasing purpose.

Next, the surface damage was removed by chemical etching, using a solution of H_2SO_4 : H_3PO_4 (3:1) at 300°C for 20 minutes, and then rinsed in DI water for 5 minutes. Then a smooth surface of the sapphire substrate was obtained through annealing at around 1400°C under air ambient. Finally, the sapphire was ready to growth after rinsing for 3 minutes in acetone, methanol, and hot aqua regia, respectively, followed by a 3-minute rinse in DI water. The ZnO films were grown in the Riber-3200 MBE system. The growth chamber was evacuated by an oil-free turbo molecular pump which produced a base vacuum of ~10^{-9} Torr.

A conventional Knudsen cell filled with pure elemental zinc was heated at high temperature to supply the zinc molecular beam flux for growth. Active oxygen source, produced by radio frequency (RF) plasma, was injected into the growth chamber via a quartz pipe, where the flow rate was controlled by a leak valve. RF plasma breaks the O_2 or N_2 bond and supplies sufficient atoms as well as ions for the deposition of oxides, nitrides or other films. Since the oxygen dissociation required much less energy than ionization (Table 2), the oxygen plasma serves as a good source of neutral monatomic oxygen. RF plasma used relative-low-frequency excitation (13.56 MHz) through an RF coil to couple energy into the plasma-discharge region, and only low-energy (<10 eV)

neutral species were allowed to escape because of the plasma sheath effect.

Table 2. Ionization/ Dissociation of O2, N2, O and N

Species	Ionization E	Dissociation E
O_2	12eV	5.2eV
O (1^{st})	13.64eV	
N_2	15.58eV	9.797eV
N (1^{st})	14.53eV	

The optical emission spectrum generated by the RF plasma contains information regarding the composition of the plasma. For O_2 plasma, the spectrum included the peaks at ultraviolet (UV), visible and infrared (IR) range. The spectra were detected by a fiber optic spectrometer which measured the plasma directly through the rear viewport of the RF plasma source. Figure 11 shows the presence of radical O* . As the pressure (O_2 flow rate) increased, the emission at 777 nm became more dominant. This emission was due to the atomic oxygen transition of $3p^5P - 3s^5S^0$ [21].

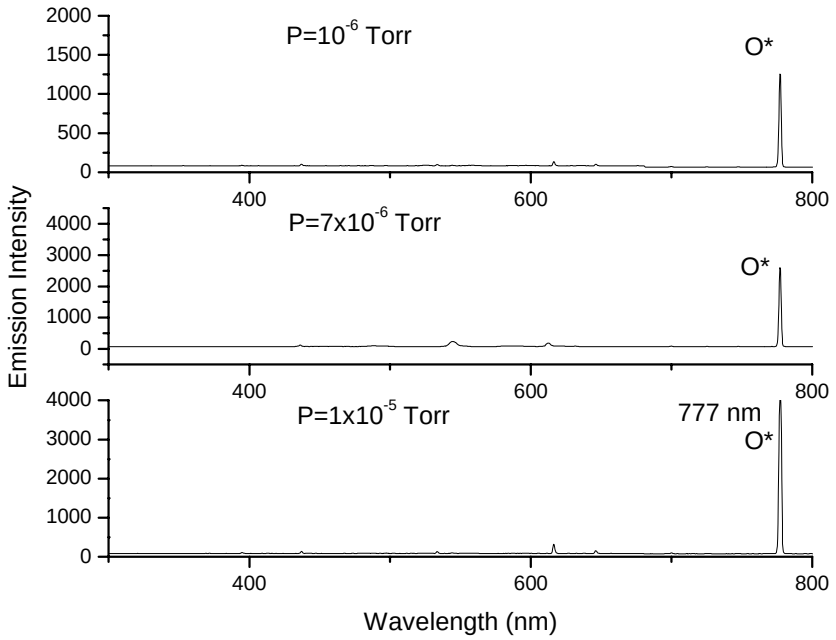

Figure 11. Optical emission spectra of the oxygen plasma at different pressure (O_2 flux flow rate). The operation power is at 350W. Pressure in the growth chamber is indicated.

In our experiments, the growth procedures were divided into four stages, as shown as Figure 12. After thermal cleaning at 700°C, the sapphire substrate generated a sharp streaky RHEED pattern with Kikuchi lines. Then the samples were treated with/without O plasma pretreatment, respectively. Next, buffer layers were deposited at low temperatures (LT) ranging from 250°C to 500°C, followed by *in-situ* annealing at a high temperature around 700°C. The annealing continued with the presence of oxygen plasma until a sharp streaky RHEED pattern occurred. Finally, ZnO films grew at high temperatures (HT) ranging from 550°C to 700°C. Table 3 lists the details of the growth on sapphire c-plane under different conditions.

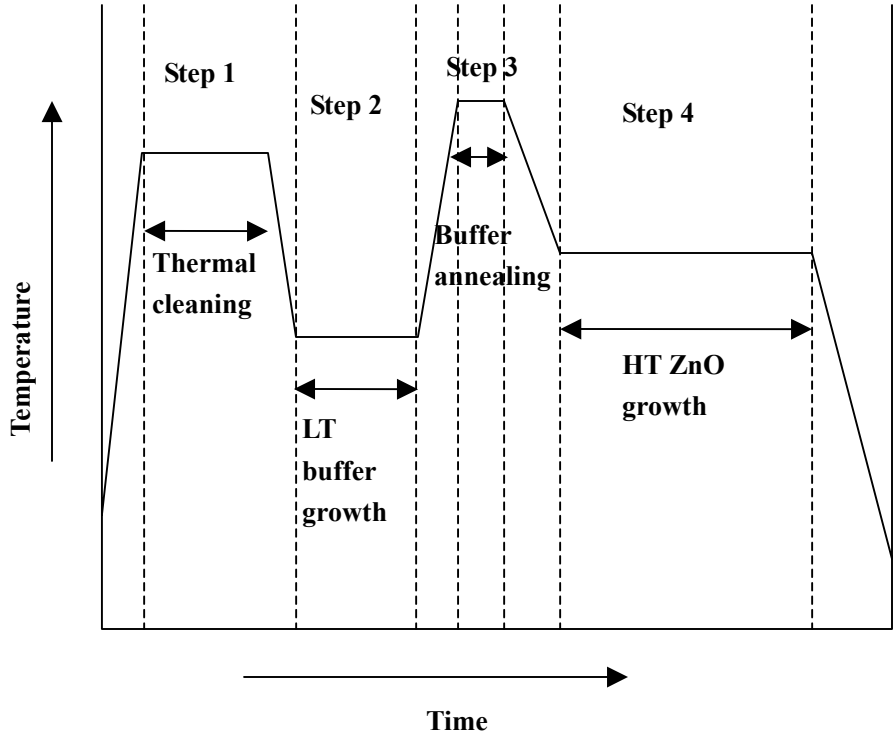

Figure 12. ZnO Growth on c-plane sapphire procedure

Table 3. ZnO sample groups grown under different conditions

HT(°C) / LT(°C)	550	600	650	700
250	146	145, 147, 148	144	149(no anneal)
300		120, 122, 123, 124, 130, 136(O* treatment at 650°C) 138, 141, 151, 152	125,126,127,128,129	121
350	134	143		
500		137		

Note: the number # in the table is sample # in the experiments.

During the growth, the oxygen pressure in the growth chamber was kept around

4×10^{-6} Torr, with RF power at 350 W. The beam of flux of Zn was usually fixed unless the optimization of the Zn flux was needed to determine the stoichiometric condition (II/VI ratio).

3.3.2 Results and discussion

The epitaxial relationship between the ZnO films and the sapphire substrate, and growth modes were studied by RHEED, AFM, SEM and PL.

3.3.2.1 Growth mode and RHEED pattern

Figure 13 shows the RHEED patterns observed during the first growth procedure. The sapphire substrate showed a sharp pattern directly after the thermal pretreatment, which indicated a clean and flat surface, as shown in Figure 13 (a). At the initial growth stage, a streaky pattern was observed, indicating a two-dimensional epitaxial growth (2D nucleation mode) despite of the large lattice mismatch (18%) as shown in Figure 13 (b). The $[2\bar{1}\bar{1}0]$ direction of ZnO aligned with the $[1\bar{1}00]$ direction of the sapphire, and the $[\bar{1}100]$ direction of the ZnO aligned with the $[1\bar{2}00]$ direction of the sapphire. This 30°C rotation can be seen from Figure 14 clearly. Due to the similarity of the symmetry, the ZnO lattice aligned itself with the oxygen sublattice in sapphire, reducing the lattice mismatch from 32% to 18%. Wang et al reported that the rotation domain and defects could be eliminated by several ways (Ga pre-exposure after O^* pretreatment or nitridation) as described in section 3.2[22, 23].

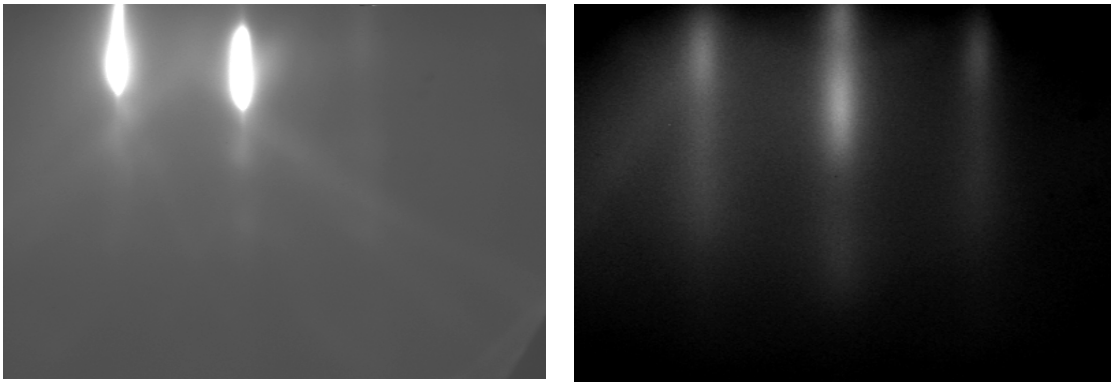

Figure 13. RHEED pattern of ZnO on sapphire (0001) plane
(a) After thermal cleaning (b)At the initial (15 sec) LT growth

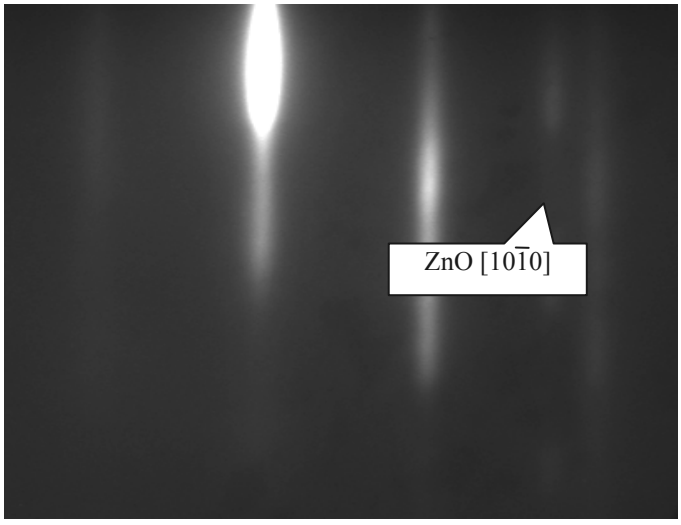

Figure 14. RHEED pattern of ZnO on sapphire with 30° rotation

Figure 15 showed the subsequent growth results. Figure 15 (a) is the RHEED pattern of ZnO films after 3 minutes growth at LT. Compared to Figure 13 (b), a gradual change occurred from the streaky pattern to a spotty one, indicating that the growth surface become rough because of the formation of islands on the growth surface, i.e., the growth

mode transitioned from 2D nucleation to 3D nucleation. This transition depends on the growth temperature. Once the thickness exceeds a critical value, the epitaxial layers relax, leading to the formation of defect free islands[21]. During the subsequent HT growth, a spotty pattern appeared to superimpose on the streaky pattern, as shown in Figure 15 (c) (after 15 seconds growth at HT), indicating the formation of islands on the growth surface. Later, the RHEED pattern became sharp and streaky again after 2 hours growth at HT (600°C), as shown in Figure 15 (d). This change was caused by the enhancement of the surface diffusion at high temperature, which prolonged the two dimensional growth and hindered the three dimension nucleation and growth.

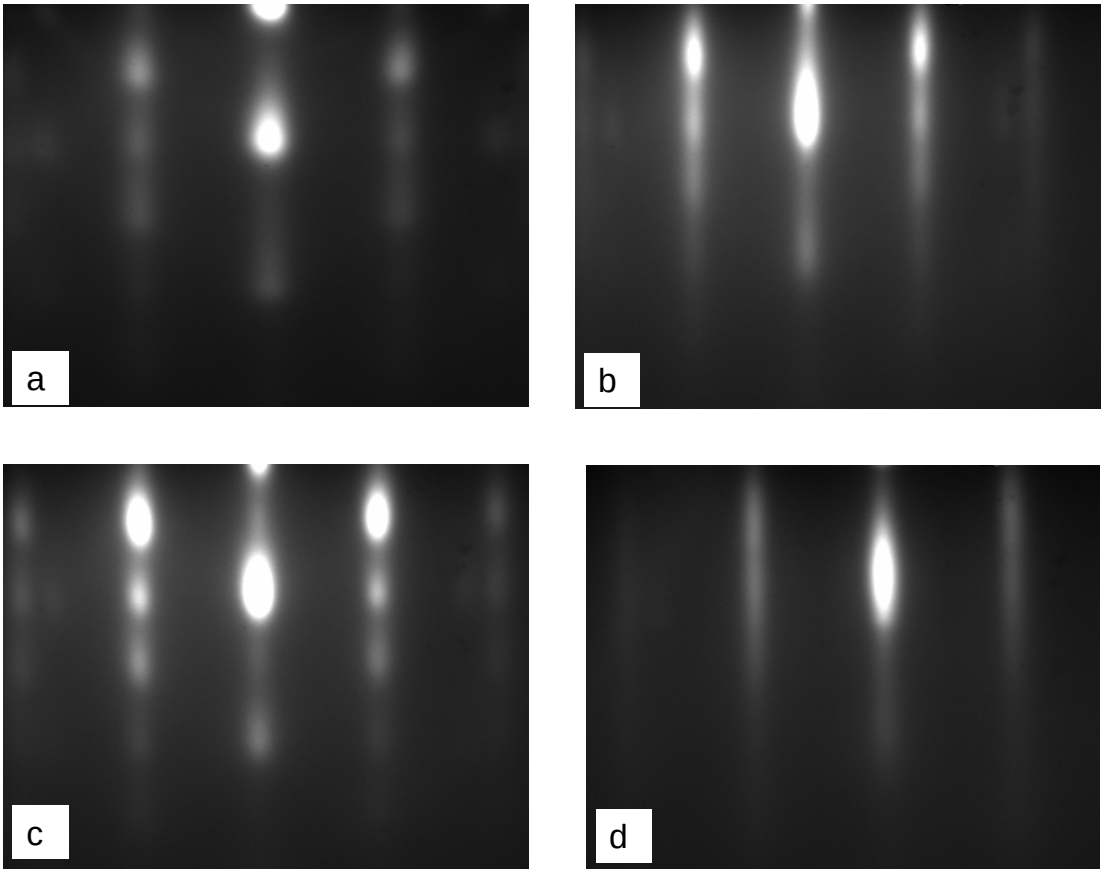

Figure 15. RHEED pattern of ZnO on sapphire (a) After LT growth (3 minutes), (b) After annealing at 700°C, (c) At the initial (30 sec) HT growth, (d) after HT growth (600°C, 2 hours)

3.3.2.2 Morphology

AFM and SEM studies on the surface morphology of the ZnO films revealed a strong dependence of the films on the growth temperature. Figure 16 shows the SEM photograph and XRD patterns of ZnO films measured in three different regions. The buffer layer was grown under LT (300°C) for 3 minutes, annealing at 700°C, then followed by HT growth at 600°C for 2 hours while zinc cell temperature was 540°C/310°C (Tip/Base), and the growth chamber pressure was kept at 4.0×10^{-6} Torr

(the oxygen flux is fixed). A rough surface consisting of crystallites was observed since the temperature profile on the substrate was not uniform and the growth temperature varied (~80°C range)in different regions from the pyrometer measurement . The RHEED pattern shows that 2D nucleation occured at the initial state. Some researcher reported that if the growth temperature was too low (less than 480°C), the initial 2D nucleation could not be formed [21]. During the subsequent 3D growth mode, at low temperature, Zn clusters could nucleate because the surplus Zn atoms might serve as the nucleation for the further formation of the ZnO crystallites. At higher temperatures, because of the competing processes of surface migration and re-evaporation, this process will be prohibited. However, due to the presence of the structural defects and incoherent boundaries of the 2D islands, the growth in 3 D mode could continue. However, if the growth temperature was too high, many flaws between the uncoalesced islands would form and lead to rough surface. Therefore, the high quality ZnO films needs to be grown at the moderated temperature. Figure 16(b) shows the films grown at the median temperature, with relatively flat surface and big grains compared to those in Figure 16(a) and (c). Figure 16 (d) shows the XRD pattern of ZnO corresponding to each region as shown in Figure 16(a)-(c). The FWHM of the rocking curve, a gauge to evaluate the crystal quality, are 14 arcmin, 7.2 arcmin and 28 arcmin respectively. This result confirmed that a moderate growth temperature is the optimum condition to grow high

crystal quality ZnO successfully. In addition, the typical $\theta - 2\theta$ scan was performed and ZnO (0002) peak at 34.6° was found.

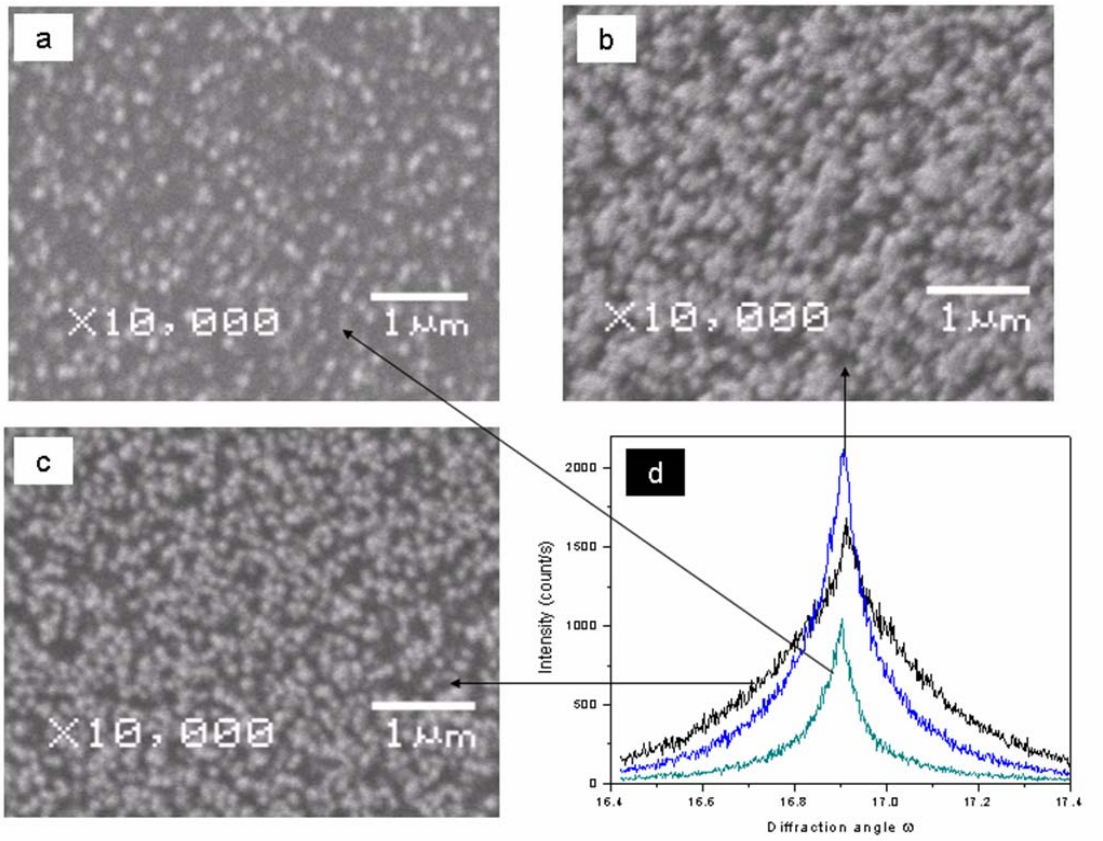

Figure 16. SEM Image and XRD pattern of ZnO measured at different regions with various temperature (a) Lower temperature (b) Middle temperature (c) High temperature (d) XRD pattern ZnO in (a), (b) and (c) region

3.3.2.3 Effect of thermal annealing of ZnO films

To improve the ZnO epi-layer quality, thermal annealing after the MBE growth was performed. The sample was followed by LT (300°C) buffer and HT (600°C) growth. The

annealing temperatures ranged from 900°C to 1050°C under air.

Figure 17 (a)-(d) show the AFM image of ZnO epi-layer (the RHEED pattern during the growth are shown at Figure 15) after annealed at 900°C, 950°C, 1000°C, and 1050°C for 1 hour, respectively. Smooth and flat surfaces were obtained after the annealing. When the annealing temperature was between 950°C and 1000°C, the best surface with regular step appeared, shown in Figure 17 (b) and (c). The increase of temperature led to an increase of the possiblity of Zn to move to the corner of irregular steps, resulting in pit formation, as shown in Figure 17 (d).

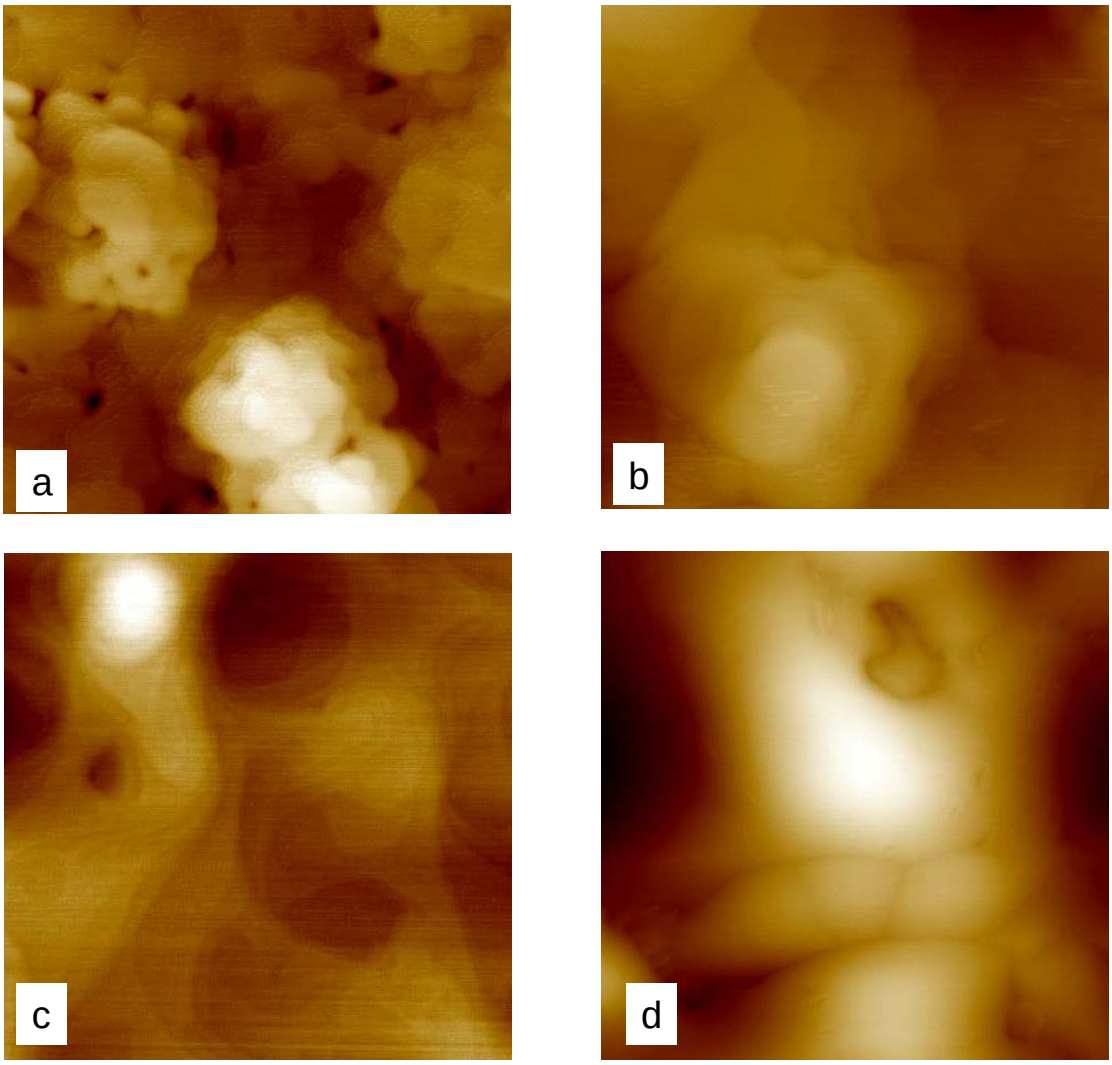

Figure 17. AFM images of 2x2 *u*m area show the surface morphology of ZnO epilayer annealed after MBE growth annealing at (a) 900°C, (b) 950°C, (c) 1000°C, (d) 1050°C under air ambient for 1 hour. The samples are grown at LT 300°C & HT 600°C.

Figure 18 shows the XRD rocking curve of annealed ZnO films. The lines in (a)-(d) correspond to samples with AFM image in Figure 17 (a)-(d) respectively. The line (e) is from the as-grown samples. It also implied that ZnO films annealed between 950°C and 1000°C had higher crystal quality, as shown in Figure 18 (b-c), confirming the results by AFM analysis.

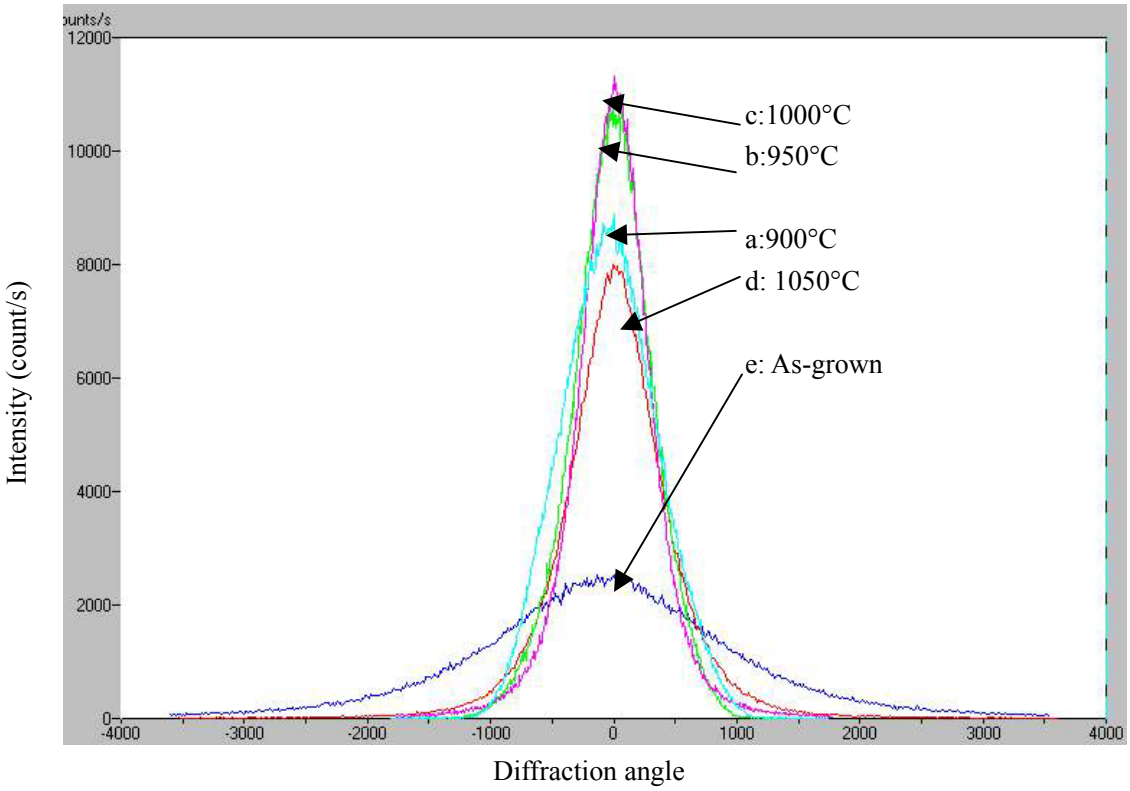

Figure 18. Rocking curve (0002) of as grwon and annealed ZnO films

Chapter 4 growth and characterization of ZnO films on epi-GaN

4.1 INTRODUCTION

Although the most common substrate for ZnO films growth is sapphire in the c-plane, which has shown promising optical and electrical properties as discussed in chapter 3, the crystal quality of the ZnO layers still needs to improve. High resolution XRD analysis indicated that the presence of degraded ZnO layers around the interface region led to the high density of defects, and the low quality interface layer was formed presumably due to the large lattice misfit (18%) between the ZnO epi-layer and the sapphire substrate. Therefore, a substitute substrate which has smaller lattice misfit for sapphire is needed.

To find the appropriate substrate, researchers have tried to grow ZnO films on a variety of material substrates, such as GaN, Si, SiC, GaAs, CaF_2 and $Sc_xMg_{1-x}AlO_4$. The materials' lattice constants and the misfits with ZnO are listed in Table 4[28].

As seen in Table 4, GaN is a closely lattice-matched material to ZnO with a lattice mismatch of only 1.8% (much less than that of the sapphire). Besides small lattice mismatch, the thermal mismatch of ZnO/GaN is also smaller than that for ZnO/sapphire. In addition, if either SiC or sapphire is used as substrates, generally the stacking

mismatch boundaries, the inversion domain boundaries, and major planar defects with stacking faults will occur on wurtzite films[29]. These will cause stacking errors due to the existence of surface steps on anisomorphic substrates. Therefore, to reduce threading plannar defects, isomorphic single crystal substrates are the best choice. Epitaxial GaN (epi-GaN) grown on sapphire can meet this requirement and now is available as substrates to grow ZnO films. In the case of ZnO / epi-GaN / nonisomorphic Al_2O_3, threading planar defects in GaN may be continued to the upper ZnO layer since the GaN

Table 4. Lattice parameters of a number of the prospective substrate materials for ZnO

Material	Crystal structure	Lattice parameters	Lattice mismatch, %	Thermal expansion coefficient, α, K-1 α_a-10^6 , α_c -·10^6
ZnO	Hexagonal	3.252, 5.213	-	2.9, 4.75
GaN	Hexagonal	3.189, 5.185	1.8	5.17, 4.55
AlN	Hexagonal	3.112, 4.980	4.5	5.3, 4.2
α-Al_2O_3	Hexagonal	4.757, 12.983	38	7.3, 8.1
α-6H-SiC	Hexagonal	3.080, 15.117	3.5	4.2, 4.68
Si	Cubic	5.430	40.1	3.59
GaAs	Cubic	5.652	42.4	6.0

layer is too thin. However, it must have lower density of threading planar defects than those produced from the direct growth of ZnO on nonisomorphic substrate[29]. Furthermore, the (0001) surfaces of ZnO and GaN are polar structure, and this polarity

has a big influence on the structure, optical and electrical properties[30]. In this study, the epi-GaN (Ga termination) grown on sapphire by metal organic chemical vapor Deposition (MOCVD) is used as the substrate to grow ZnO epi-layer. The thickness of epi-GaN is about 2 um.

4.2 EXPERIMENTAL PROCEDURES

Same as the growth of ZnO films on sapphire, a typical Knudsen effusion cell was used to evaporate zinc source. Atomic oxygen was produced by RF plasma source. The background pressure of the growth chamber before introduction of oxygen was around $\sim 10^{-8} Torr$.

After the conventional cleaning, prior to growth, the substrate was taken thermal cleaning at around 650°C. Series of different pre-treatments were performed as follows:

1. The first group samples. First RF plasma was stablized for typically about 2-3 minutes. During the stabilization, oxygen gas was supplied into the chamber with the oxygen shutter closed. Then when RF plasma was stable, the zinc and oxygen shutters were opened at the same time for ZnO film to grow. This batch of specimens was called oxygen pre-exposed samples.

2. The second group samples. At first, after the thermal cleaning, the substrate was exposed to zinc flux for 2-3 minutes and the oxygen plasma was ignited and stabilized. During the plasma stabilization, zinc exposure to the substrate was sustained. After the

RF plasma became stable, the oxygen shutter was opened immediately. This group was called zinc pre-exposure samples.

After the pretreatments, a ZnO buffer layer was deposited at relatively low temperatures ranging from 280°C to 350°C. Then ZnO buffer was annealed at around 600°C (we tried the range from 300°C to 700°C) to improve the surface until a streak pattern monitored by *in-situ* RHEED was obtained. Subsequently, ZnO films were grown in a temperature range from 600°C to 700°C while the growth rate was between 0.2-0.5 *u*m/h. During the growth, the oxygen flow rate was kept constant at 0.7 sccm, with a fixed working pressure at around $4x10^{-6}$ Torr.

4.3 RESULTS AND DISCUSSIONS

As shown in Figure 19 (a), a sharp and streaky RHEED pattern of the epi-GaN surface after thermal cleaning indicated a well ordered and flat surface. The pattern changed a little bit when the epi-GaN was exposed to oxygen plasma at low temperature (300°C), and became diffusive and finally disappeared after long time exposure to oxygen at a high temperature (600°C),as shown in Figure 19 (a). This change was presumably attributed to the epi-GaN surface oxidation which led to the disordered epi-GaN surface. This oxidized and disordered epi-GaN surface might be the reason that the ZnO films grown on O-exposed epi-GaN showed degraded quality. On the contrary, the pre-exposure of epi-GaN to Zn was found to be very effective to improve the quality

of ZnO films.

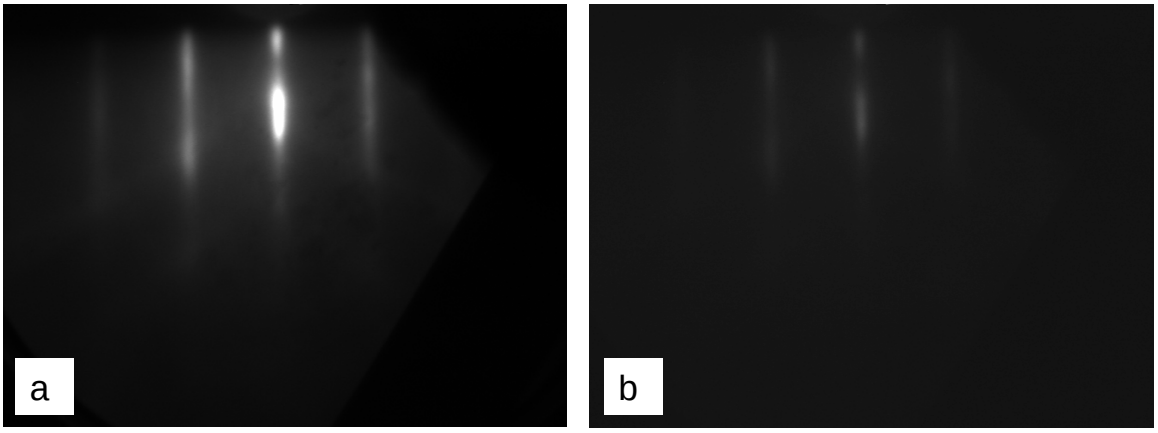

Figure 19. RHEED pattern of ZnO growth on epi-GaN (a) After thermal cleaning (b) RHEED pattern disappearing after O exposure

4.3.1 Buffer layer optimization

An appropriate buffer layer growth at low temperature is a crucial process for ZnO epitaxial growth on epi-GaN substrate. The buffer layer will adapt lattice strain through annealing, which is necessary for subsequent ZnO growth with flat surface. Another purpose of this low temperature buffer layer is to reduce the reaction of oxygen atoms with Ga-terminated epi-GaN surface.

Figure 20 (a)-(f) show the RHEED patterns before and after annealing at various temperatures from 300°C to 700°C, with the thickness of the buffer around 10 nm. The RHEED pattern of the low temperature buffer was composed of diffused streaks and elongated spots, indicating that the surface of the buffer layer was characterized by small

two dimensional islands compared to that with the long streaky beam. This change of RHEED patterns from diffused streaks with elongated spots into a little more clear elongated spots occurred during annealing at 300°C, as shown in Figure 20

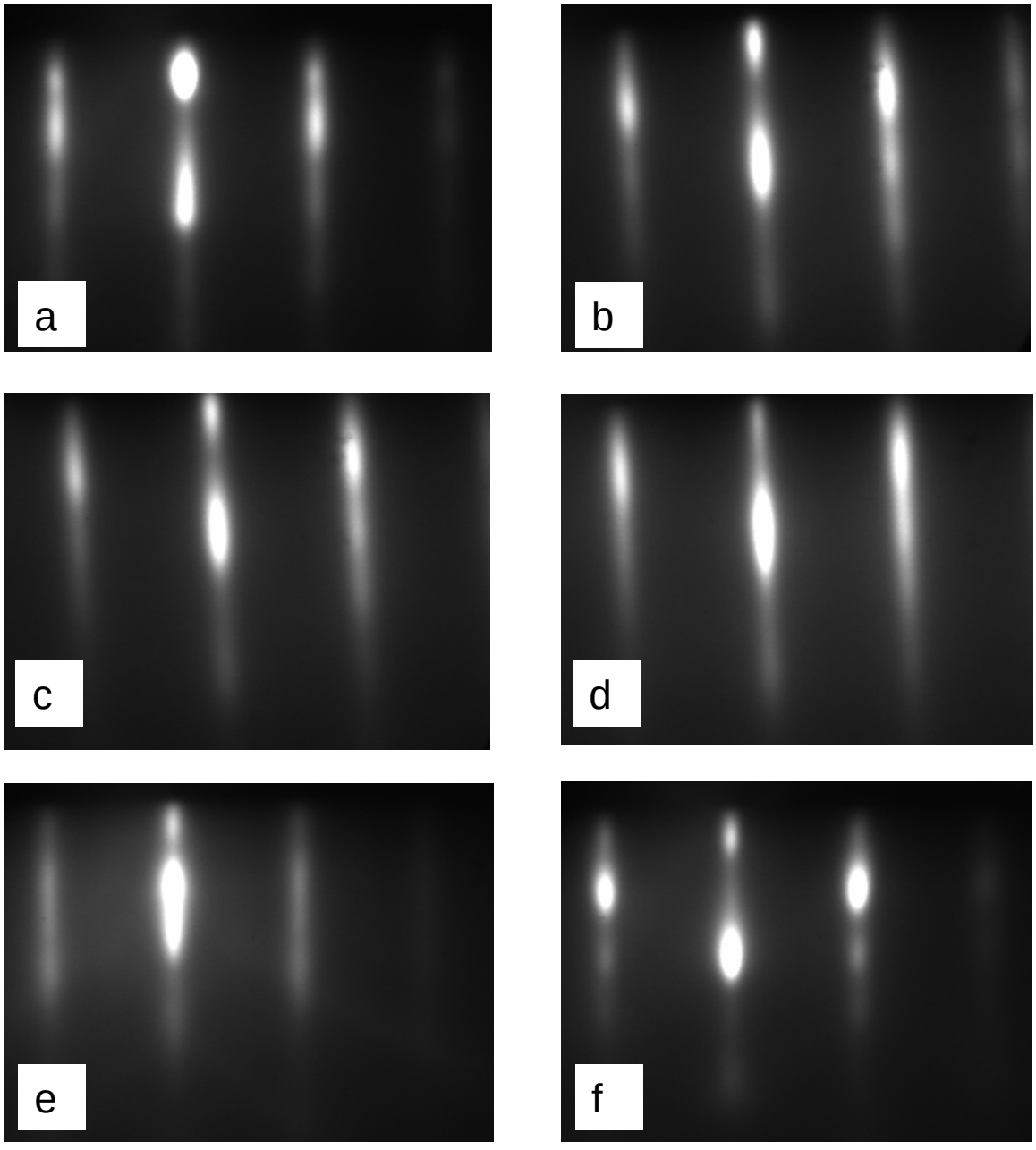

Figure 20. RHEED pattern of ZnO growth on epi-GaN (a) After LT buffer growth at 250°C, (b) After buffer annealing at 300°C, (c) After buffer annealing at 400°C, (d) After buffer annealing at 600°C, (e) After buffer annealing at 650°C, (f) After buffer annealing at 700°C

(b). As the temperature increased, the RHEED pattern became more streaky and longer, which implied that the surface was reconstructed to an extended island surface with improved lattice ordering. The best result was obtained during annealing at 600°C, as shown in Figure 20 (d), which produced a smooth and high quality ZnO surface from the RHEED pattern.

At high temperature, the RHEED pattern maintained a streaky pattern during ZnO growth. This evolution of the RHEED patterns indicated a transition in the growth mode from layer by layer to step-flow growth, which is necessary for growing the high quality of ZnO films.

However, when the temperature was greater than 650°C, the RHEED pattern changed back to the diffuse and spotty pattern. This is ascribed to the oxidized and disordered epi-GaN surface, especially when buffer layer thickness was too thin.

To explore the growth of the buffer layer, several samples were grown only at LT. The same growth procedures were used as described in section 4.2. The substrate was a 2 μm thick epi-GaN layer grown by MOCVD. After the conventional chemical and thermal cleaning of the GaN substrate, ZnO layers were grown at 250°C while zinc cell temperature was kept at 500°C/300°C (tip/bottom). RF plasma source worked at 350W

with a vacuum of 4×10^{-6} Torr. The thickness of the ZnO layer is around 20nm. Then the substrate temperature was increased to 600°C for annealing for about 3 minutes under oxygen ambient.

Figure 21 shows the AFM images of the sample after LT growth and annealing. The RHEED pattern appeared as streaky elongated spots. Surface morphology experienced a remarkable change at different annealing temperatures compared to the morphology for other samples. The flat surface and large step morphology appeared after the annealing. For the samples annealed at 600°C, good surface as produced (Figure 21), and the root mean square (RMS) value of the surface roughness (describing the height different between top and bottom of the large steps) was 0.89 nm which. The smaller the RMS of the surface roughness, the flatter the surface.

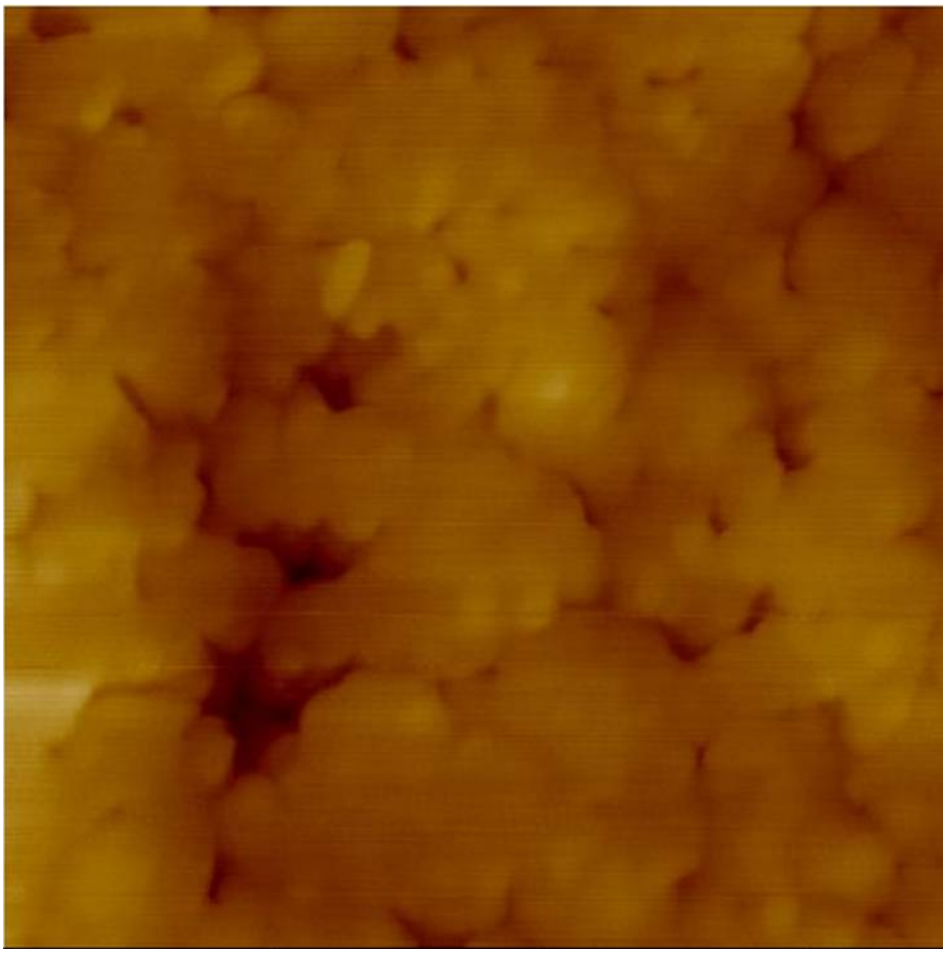

Figure 21. AFM images show the surface morphology in 2X2 μ m area of ZnO LT buffer layer

In summary, annealing played an important role in improving the morphology of the buffer layer of the ZnO films.

4.3.2 Growth temperature optimization

Another factor affecting the crystal quality of ZnO films is the growth temperature, which plays an important role in the reaction between the emitted molecules and the

substrate, including adsorption, migration on the substrate surface, interaction with other atoms, incorporation into the crystal, and desorption. During the growth, the substrate was heated to such a high temperature that the arriving Zn and O atoms had sufficient energy to move around on the surface and to deposit on their correct bonding positions. However, if the temperature is too high, these atoms may be re-evaporated from the surface, leading to low growth rate.

Figure 22 and Figure 23 show the surface morphologies of ZnO films grown at different temperatures observed by AFM in $2\mu m \times 2\mu m$ or $5\mu m \times 5\mu m$ areas, respectively. Except the substrate temperature, all the other growth parameters are the same. The buffer layers grown at 250°C exhibited a sharp streaky RHEED pattern. As shown in Figure 22 and Figure 23, the surface morphology was significantly different, and the ZnO surface became rougher with the increasing growth temperature. When the growth temperature reached 650°C and 700°C, AFM $2\mu m \times 2\mu m$ images could not be obtained, and instead the $5\mu m \times 5\mu m$ images were used. The large flat morphology steps were observed for the sample grown at 600°C.

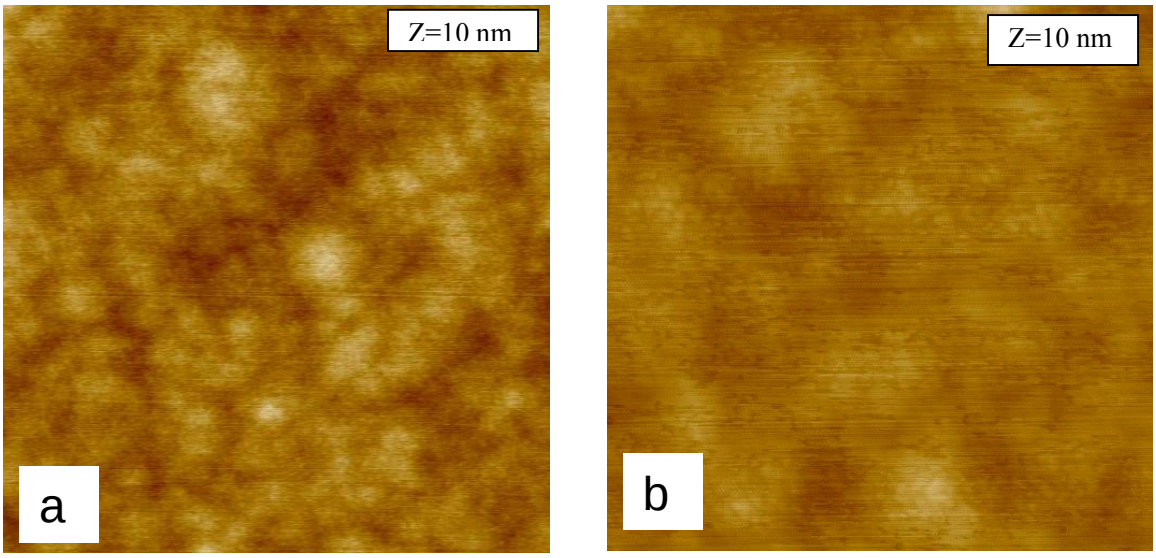

Figure 22. AFM images show the surface morphology in 2X2 μ m of ZnO grown on epilayer GaN at (a) 500°C, (b) 600°C

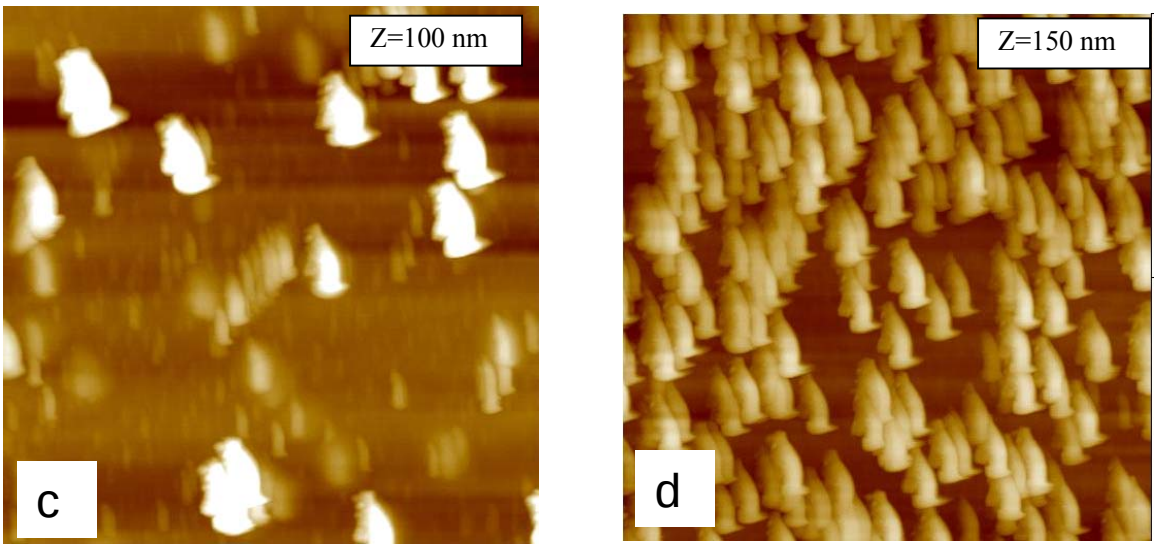

Figure 23. AFM images show the surface morphology in 5x5 μ m area of ZnO grown on epilayer GaN at (a) 650°C, (b) 700°C

4.3.3 XRD analysis

The radial scans (ω-2θ) and rocking scans (ω) were measured for samples grown in

different conditions.

Figure 24 shows the XRD curve of (ω-2θ) scan around the (0002) lattice plane. This 0.9 μm thick ZnO layer was grown at 600°C with base temperature at 500/320°C and oxygen plasma flux of 0.6 sccm. Because the 2θ positions of ZnO and GaN are very close to each other (for an ideal ZnO 2θ: 34.406°, GaN 2θ: 34.598°), the overlap of the GaN and ZnO peaks are shown in the Figure 24, displaying a Lorentzian line shape and this curve can be fitted with two peaks in the figure. The peaks at 34.55° (FWHM=5.3 arcmin) and 34.67° (FWHM=5.5 arcmin) are from ZnO and GaN respectively. From the positions of the peaks, the c lattice constants were calculated by Bragg Law and they are 5.17nm and 5.05nm respectively.

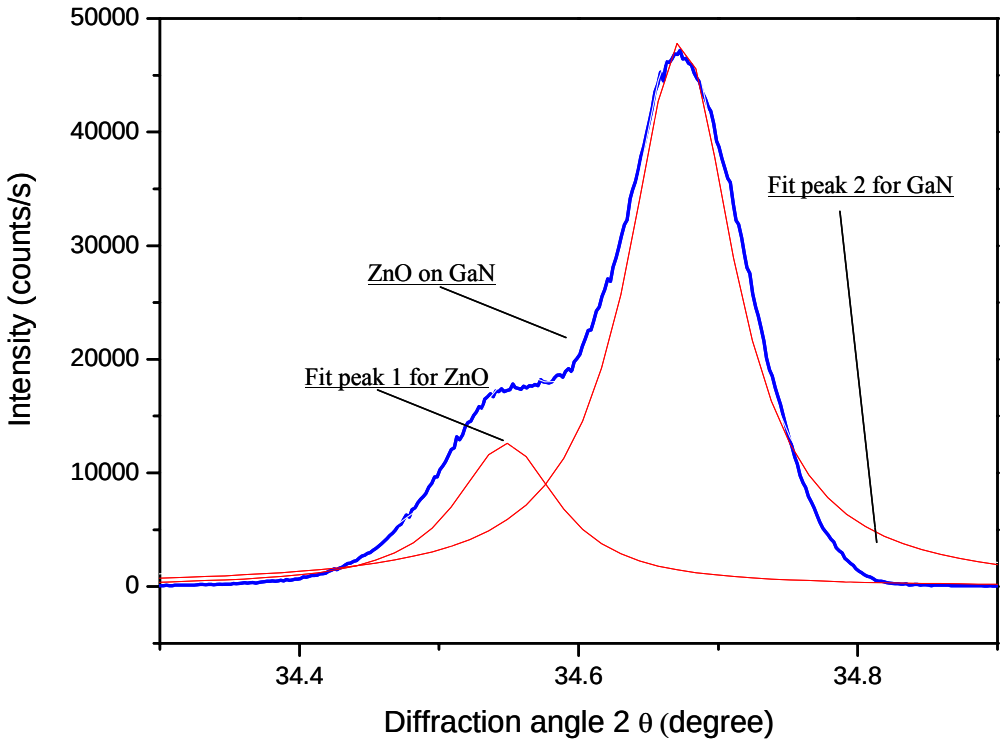

Figure 24. θ-2θ curve of a ZnO film grown on epi-GaN and two fit peaks according to Lorentzian distribution

The XRD curve of ZnO grown on GaN and the curve of substrate GaN grown by MOCVD were put together, as shown in Figure 25. The peak of GaN in Figure 25 and the fitted peak 2 in Figure 24 had the same shape and intensity, which indicated the Lorentzian fitting in Figure 24 was correct.

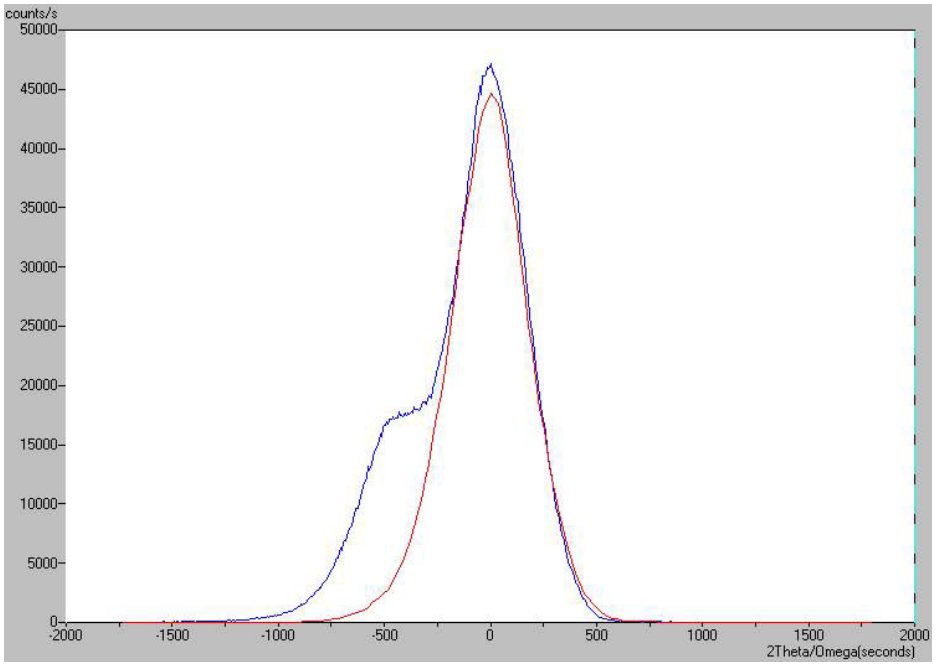

Figure 25. ZnO epi-layer and GaN substrate's XRD θ-2θ curve

The 2θ positions of ZnO and GaN are too close to each other and the resolution of FWHM is not small enough to separate the materials if the (002) lattice plane is scanned. Instead, the (102) lattice plane was scanned, showing the in-plane dislocation and the (002) plane scanning showed the inter-planar information. Figure 26 shows the XRD curve of (ω-2θ) scan around the (102) lattice plane. The ZnO and GaN peaks were separated completely.

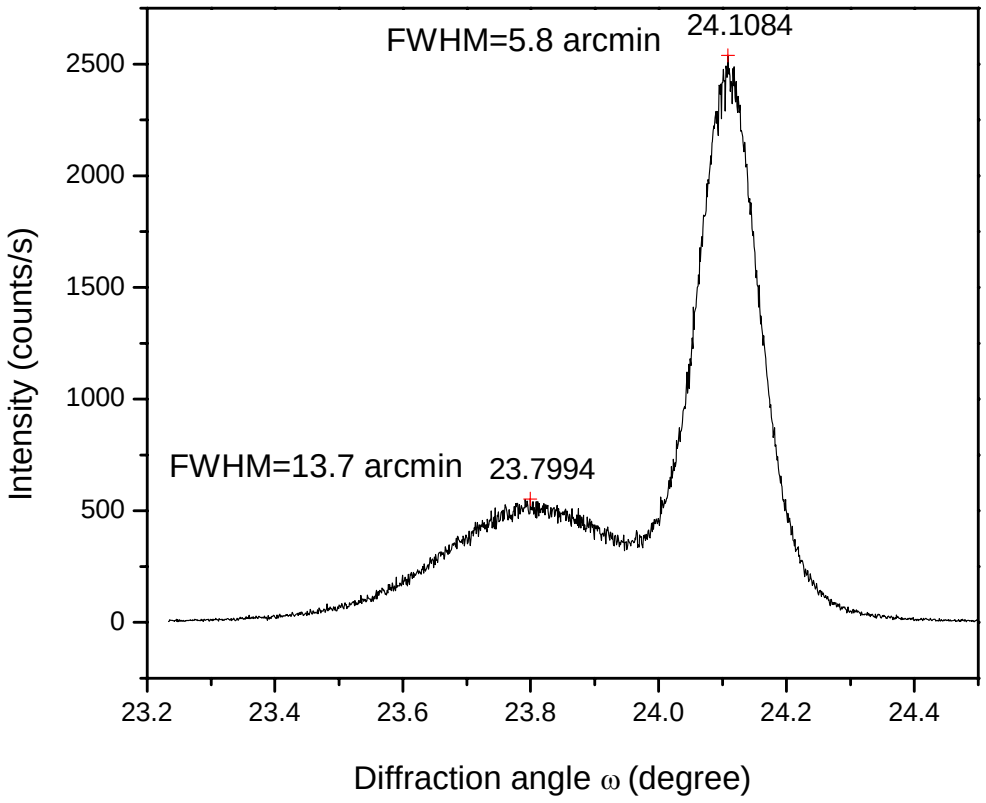

Figure 26. θ-2θ curve of annealed ZnO films scanned along (102) direction

4.3.4 Photoluminescence and optical properties analysis

Figure 27 and Figure 28 show PL spectra of ZnO at room temperature. Figure 27 and Figure 28 show the broad peaks about 150 meV at 3.2 eV due to the increase of the free exciton emission with the temperature. Figure 29 shows the PL spectra at a typical low temperature (T=15K). The primary characters of PL spectra can be divided into three categories: the near band edge emission, the low energy tail extending from the near band edge emission, and the deep level emission[31].

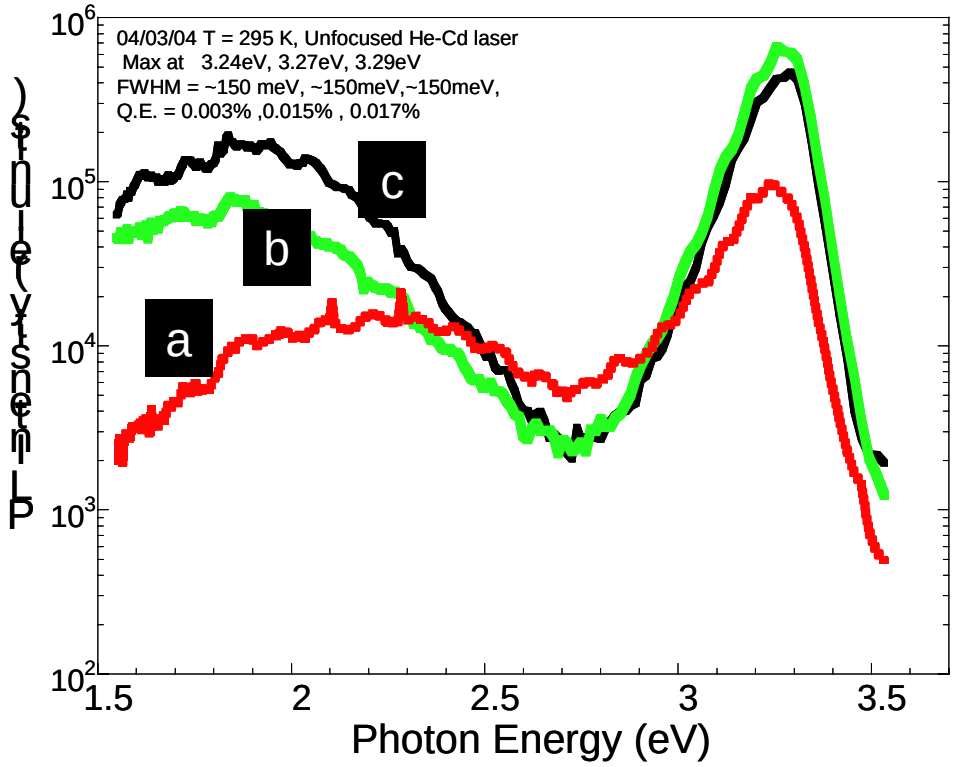

Figure 27. PL spectra of ZnO films grown on epi-GaN at different growth temperature (a) 800°C (b) 600°C (c) 650°C

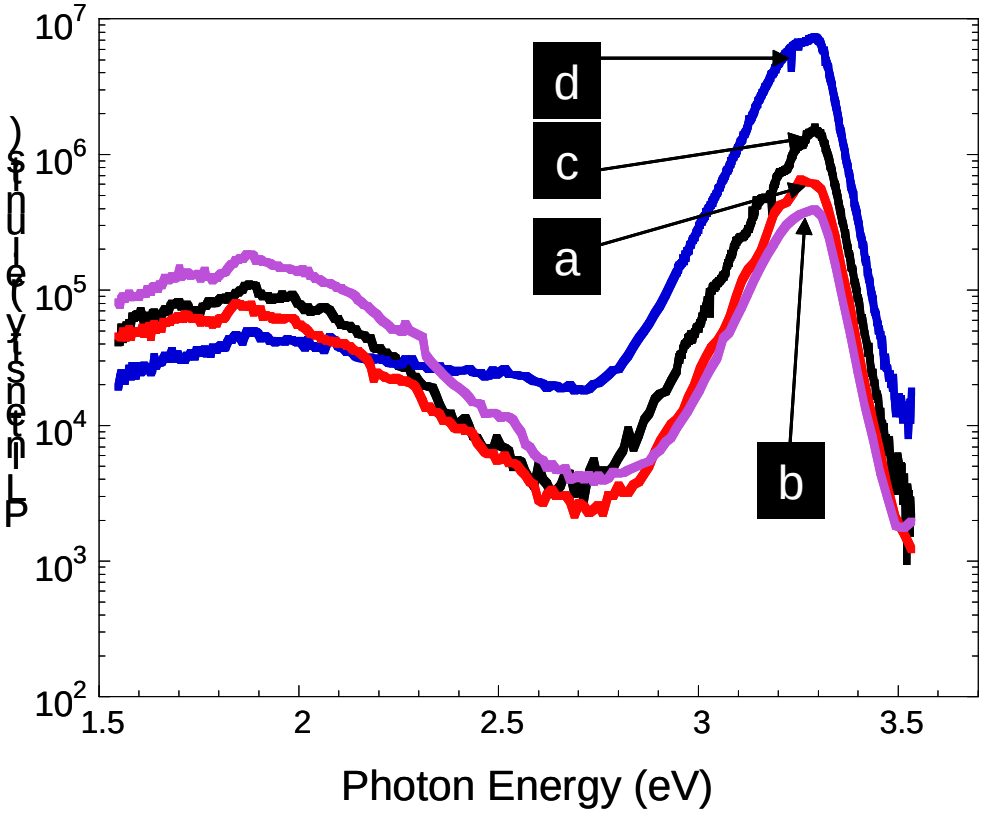

Figure 28. PL spectra of ZnO films grown on epi-GaN at different zinc flux (Zn cell base temperature) at (a) 280°C (b) 290°C (c) 300°C (d) 320°C

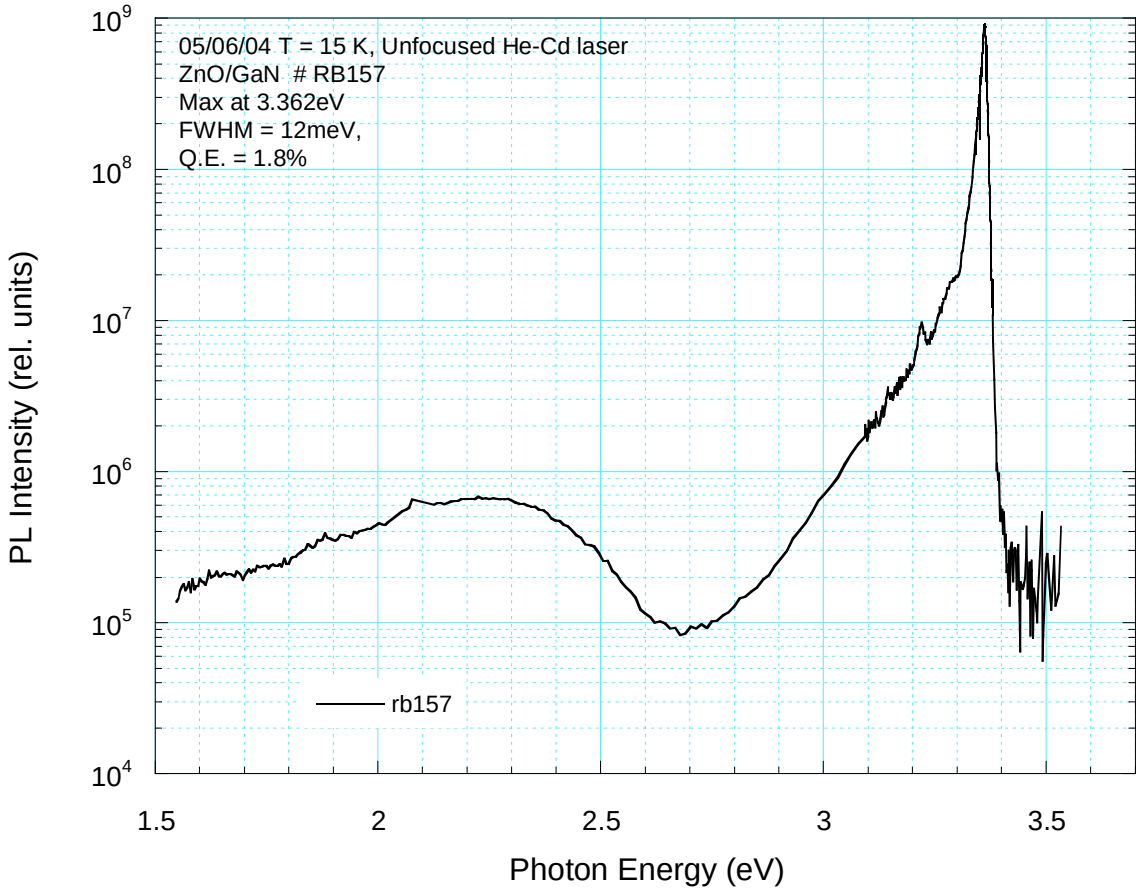

Figure 29. PL spectra(measured at 15k) of ZnO films grown on epi-GaN

Comparing the Figure 27 (a), (b) and (c), we found that at the samples grown at too high temperature resulted in poor crystal quality. Appropriate moderate growth temperature is needed to grow high quality ZnO, confirmed by the XRD results and AFM analysis. Figure 28 shows the trend change with Zinc flux (II/VI ratio).

Figure 29 shows the PL spectra of the ZnO film (same as the sample in Figure 24 of XRD analysis) measured at 15K, showing a strong near band edge emission at 3.362 eV with FWHM of 12 meV. This peak was due to the recombination of exciton bound to

neutral donors or acceptors[1, 32]. A broad deep emission was observed around 2.3 eV, which was thought to come from the transition from conduction band or shallow donor band to deep acceptor band due to the energy level of vacancy of Zn or oxygen.

Conclusion

ZnO single crystal films were grown on sapphire (0001) and epi-GaN by oxygen plasma assisted MBE, respectively. Suitable pre-growth treatments were developed for substrate cleaning. Various pretreatments including the oxygen or Zn pre-exposure gave different effects to buffer layers and the growth of ZnO at high temperature (HT). Then the crystalline quality and optical properties of the ZnO films were characterized by XRD, AFM, SEM and PL.

For the growth on both substrates, the in-situ RHEED observations showed a 3D growth mode after a transition from an initial 2D growth. Then the rotation domains, growth mode, surface morphology and crystal quality were analyzed. These results revealed that for the growth of ZnO films on sapphire, the $[2\bar{1}\bar{1}0]$ direction of ZnO aligns with the $[1\bar{1}00]$ direction of the sapphire, and the $[\bar{1}100]$ direction of the ZnO aligns with the $[11\bar{2}0]$ direction of the sapphire, thereby producing a 30°C rotation which reduced the lattice mismatch from 32% to 18%.

As to the growth of ZnO films on GaN substrate, the effects of the buffer layer, II/VI flux ratio and growth temperature were studied. The ZnO epilayers grown under stoichiometric flux condition and at moderate temperatures had a higher crystalline quality. The buffer layer is crucial to grow high quality ZnO films. After the deposition

of the buffer layer at LT (~300°C followed by annealing at 700°C for growth on sapphire, ~280°C followed by annealing at <700°C for growth on GaN), and the RHEED showed a sharp and streaky pattern which indicated a flat surface and a higher quality, subsequently confirmed by XRD and PL investigations. The FWHM of ZnO films grown on sapphire was about 7.2 arcmins. For the ZnO grown on GaN, the ZnO and GaN peaks separated completely while scanning around (102) lattice plane, and the peaks positions were at 23.8° and 24.1°, respectively. The curve scanned around (002) can be fitted into two peaks according the Lorentzian distribution. The PL spectra of ZnO film grown on GaN measured at 15K exhibited a strong near band edge emission at 3.362 eV with FWHM of 12 meV due to the recombination of exciton bound to neutral donors or acceptors. A broad deep emission was observed around 2.3 eV, which was assigned to the transition from conduction band or shallow donor band to deep acceptor band due to the energy level of vacancy of Zn or oxygen.

In addition, the effects of thermal annealing of ZnO films were investigated. The results revealed that the crystalline quality was improved after annealing, and the best results occurred at temperatures range from 950°C to 1000°C.

In conclusion, MBE can provide high quality to the ZnO films for application to optoelectronic devices.

List of references

List of references

[1] D. C. Reynolds, C. W. Litton, and T. C. Collins, "Zeeman Effects in Edge Emission and Absorption of Zno," *Physical Review*, vol. 140, pp. 1726-1734, 1965.

[2] Z. K. Tang, G. K. L. Wong, P. Yu, M. Kawasaki, A. Ohtomo, H. Koinuma, and Y. Segawa, "Room-temperature ultraviolet laser emission from self-assembled ZnO microcrystallite thin films," *Applied Physics Letters*, vol. 72, pp. 3270-3272, 1998.

[3] D. M. Bagnall, Y. F. Chen, Z. Zhu, T. Yao, S. Koyama, M. Y. Shen, and T. Goto, "Optically pumped lasing of ZnO at room temperature," *Applied Physics Letters*, vol. 70, pp. 2230-2232, 1997.

[4] C. F. Walters, K. F. McCarty, E. A. Soares, and M. A. Van Hove, "The surface structure of [alpha]-Al2O3 determined by low-energy electron diffraction: aluminum termination and evidence for anomolously large thermal vibrations," *Surface Science*, vol. 464, pp. L732-L738, 2000.

[5] A. Tiwari, C. Jin, J. Narayan, and M. Park, "Electrical transport in ZnO[sub 1 - delta] films: Transition from band-gap insulator to Anderson localized insulator," *Journal of Applied Physics*, vol. 96, pp. 3827-3830, 2004.

[6] R. P. S. Chakradhar, B. M. Nagabhushana, G. T. Chandrappa, K. P. Ramesh, and J. L. Rao, "Solution combustion derived nanocrystalline Zn[sub 2]SiO[sub 4]:Mn phosphors: A spectroscopic view," *The Journal of Chemical Physics*, vol. 121, pp. 10250-10259, 2004.

[7] X. W. Sun, S. F. Yu, C. X. Xu, C. Yuen, and B. J. Chen, "UV light source from a zinc oxide microtube," *Journal of the Society for Information Display*, vol. 12, pp. 505-508, 2004.

[8] M. H. Huang, S. Mao, H. Feick, H. Yan, Y. Wu, H. Kind, E. Weber, R. Russo, and P. Yang, "Room-Temperature Ultraviolet Nanowire Nanolasers," *Science*, vol. 292, pp. 1897-1899, 2001.

[9] L. I. Berger, *Semiconductor Materials*: CRC Press, 1997.

[10] D. P. Norton, Y. W. Heo, M. P. Ivill, K. Ip, S. J. Pearton, M. F. Chisholm, and T. Steiner, "ZnO: growth, doping & processing," *Materials Today*, vol. 7, pp. 34-40, 2004.

[11] J. A. A. Cho, "Molecular Beam Epitaxy," *Prog. Solid-State Chem*, pp. 157-191, 1975.

[12] H. Morkoc, *Nitrides Semiconductors and Devices*: Springer Verlag, 1999.

[13] M. A. Herman, SItter, A, *Molecular Beam Epitaxy*: Springer, 1989.

[14] H. Kato, M. Sano, K. Miyamoto, and T. Yao, "Effect of O/Zn flux ratio on crystalline quality of ZnO films grown by plasma-assisted molecular beam epitaxy," *Japanese Journal of Applied Physics Part 1-Regular Papers Short Notes & Review Papers*, vol. 42, pp. 2241-2244, 2003.

[15] H. J. Ko, T. Yao, Y. F. Chen, and S. K. Hong, "Investigation of ZnO epilayers grown under various Zn/O ratios by plasma-assisted molecular-beam epitaxy," *Journal of Applied Physics*, vol. 92, pp. 4354-4360, 2002.

[16] H. Ju Ko, Y. Chen, S. Ku Hong, and T. Yao, "MBE growth of high-quality ZnO films on epi-GaN," *Journal of Crystal Growth*, vol. 209, pp. 816-821, 2000.

[17] B. K. T. D. Keith Bowen, *High Resolution X-ray Diffractometry and Topography*: Taylor & Francis, 1998.

[18] T. J. Godin and J. P. Lafemina, "Atomic and Electronic-Structure of the Corundum (Alpha-Alumina)(0001) Surface," *Physical Review B*, vol. 49, pp. 7691-7696, 1994.

[19] R. Di Felice and J. E. Northrup, "Theory of the clean and hydrogenated Al2O3(0001)-(1 x 1) surfaces," *Physical Review B*, vol. 60, pp. R16287-R16290, 1999.

[20] P. D. Tepesch and A. A. Quong, "First-principles calculations of [alpha] -alumina (0001) surfaces energies with and without hydrogen," *Physica Status Solidi B*, vol. 217, pp. 377-387, 2000.

[21] Y. F. Chen, D. M. Bagnall, H. J. Koh, K. T. Park, K. Hiraga, Z. Q. Zhu, and T. Yao, "Plasma assisted molecular beam epitaxy of ZnO on c-plane sapphire: Growth and characterization," *Journal of Applied Physics*, vol. 84, pp. 3912-3918, 1998.

[22] I. Ohkubo, Y. Matsumoto, A. Ohtomo, T. Ohnishi, A. Tsukazaki, M. Lippmaa, H. Koinuma, and M. Kawasaki, "Investigation of ZnO/sapphire interface and formation of ZnO nanocrystalline by laser MBE," *Applied Surface Science*, vol. 159-160, pp. 514-519, 2000.

[23] M. Ying, X. Du, Z. Mei, Z. Zeng, H. Zheng, Y. Wang, J. Jia, Z. Zhang, and Q. Xue, "Effect of sapphire substrate nitridation on the elimination of rotation domains in ZnO epitaxial films," *Journal of Physics D: Applied Physics*, vol. 37, pp. 3058, 2004.

[24] X. L. Du, M. Murakami, H. Iwaki, and A. Yoshikawa, "Complete elimination of multi-angle rotation domains in ZnO epilayers grown on (0001) sapphire substrate," *Physica Status Solidi a-Applied Research*, vol. 192, pp. 183-188, 2002.

[25] X. Q. Wang, H. Iwaki, M. Murakami, X. L. Du, Y. Ishitani, and A. Yoshikawa, "Molecular beam epitaxy growth of single-domain and high-quality ZnO layers on Nitrided (0001) sapphire surface," *Japanese Journal of Applied Physics Part 2-Letters*, vol. 42, pp. L99-L101, 2003.

[26] S.-K. Hong, T. Hanada, Y. Chen, H.-J. Ko, T. Yao, D. Imai, K. Araki, and M. Shinohara, "Control of polarity of heteroepitaxial ZnO films by interface engineering," *Applied Surface Science*, vol. 190, pp. 491-497, 2002.

[27] A. Y. Cho and J. R. Arthur, "Molecular beam epitaxy," *Progress in Solid State Chemistry*, vol. 10, pp. 157-191, 1975.

[28] H. Morkoc, "A comprehensive review of ZnO and related devices," *Journal of Applied Physics Reviews*, To be published.

[29] S.-K. Hong, H.-J. Ko, Y. Chen, T. Hanada, and T. Yao, "Control and characterization of ZnO/GaN heterointerfaces in plasma-assisted MBE-grown ZnO films on GaN/Al2O3," *Applied Surface Science*, vol. 159-160, pp. 441-448, 2000.

[30] S.-K. Hong, H.-J. Ko, Y. Chen, T. Hanada, and Takafumi Yao, "Evolution of initial layers of plasma-assisted MBE grown ZnO on GaN/sapphire," *Journal of Crystal Growth*, vol. 214-215, pp. 81-86, 2000.

[31] Y. Chen, D. Bagnall, and T. Yao, "ZnO as a novel photonic material for the UV region," *Materials Science and Engineering B*, vol. 75, pp. 190-198, 2000.

[32] D. M. Bagnall, Y. F. Chen, M. Y. Shen, Z. Zhu, T. Goto, and T. Yao, "Room temperature excitonic stimulated emission from zinc oxide epilayers grown by plasma-assisted MBE," *Journal of Crystal Growth*, vol. 184-185, pp. 605-609, 1998.